2011

Core-Shell Nanofibres for Heart Valve Leaflet Tissue Engineering

Erica E.M. Lee

Core-Shell Nanofibres for Heart Valve Leaflet Tissue Engineering

(Thesis format: Monograph)

by

Erica E.M. Lee

Graduate Program in Biomedical Engineering

A thesis submitted in partial fulfillment
of the requirements for the degree of
Master of Engineering Science

The School of Graduate and Postdoctoral Studies
The University of Western Ontario
London, Ontario, Canada

THE UNIVERSITY OF WESTERN ONTARIO

School of Graduate and Postdoctoral Studies

CERTIFICATE OF EXAMINATION

Joint Supervisor

Dr Wankei Wan

Joint Supervisor

Dr Derek Boughner

Supervisory Committee

Dr Jeff Hutter

Dr Ray Guo

Examiners

Dr Aaron Fenster

Dr Ray Guo

Dr Andrew Hrymak

The thesis by

Erica E.M. Lee

Entitled:

Core-Shell Nanofibres for Heart Valve Leaflet Tissue Regeneration

is accepted in partial fulfillment of the
requirements for the degree of
Master of Engineering Science

Date_____

Chair of the Thesis Examination Board

ABSTRACT

The aortic heart valve regulates blood flow as it exits the heart and enters the body; when this valve malfunctions it creates serious health problems. While current valve replacement options are satisfactory, the ultimate goal is to create a living valve replacement that can self repair, regenerate and remodel as the patient grows. An approach is via tissue engineering, which uses principles from engineering and cell biology to create functional tissue substitutes for *in vivo* replacement. This study aims at fabricating nanofibrillar scaffolds by coaxial electrospinning for the treatment of valvular disease. Many electrospun biopolymers promote cell adhesion, but lack the necessary signals that encourage cell proliferation and migration. The objectives of this work are to create a bioactive scaffold by encapsulating therapeutic proteins within a polymer shell and to analyze the protein release kinetics. By incorporating growth factors into the nanofibres, controlled release within the scaffold may be achieved and biochemical cues for tissue regeneration can be signaled. Samples were analyzed using scanning electron microscopy, transmission electron microscopy and laser scanning confocal microscopy. Core-shell nanofibres composed of poly(caprolactone) (PCL) and encapsulated bovine serum albumin (BSA) were successfully prepared and had an average diameter of diameter of 1069 ± 388 nm. Electrospun PCL-BSA scaffold containing 62.7 ± 5.7 μg of BSA were able to release 35.33 ± 2.23 % of the theoretical loaded protein over 10 days. Furthermore, a method for isolating and purifying type I collagen from rat tails was developed and solid collagen fibres were prepared with an average diameter of 256 ± 48 nm. Core-shell nanofibres composed of type I collagen and encapsulated BSA with average inner and outer fibre diameters of 87 ± 33 nm and 204 ± 73 nm, respectively.

Keywords: aortic heart valve, tissue engineering, coaxial electrospinning, controlled release, poly (ε-caprolactone), type I collagen

ACKNOWLEDGMENTS

First and foremost I would like to thank my supervisors Dr Wankei Wan and Dr Derek Boughner for their encouragement and support over the last two years. I know that working with them has had a profound influence on how I approach tasks in life. I would like to thank Dr Wan in particular for his support during my medical school applications and how encouraging he was of my decision to go into the medical field. Dr Wan has been a mentor to me in so many ways, especially during our long afternoon chats. I would also like to thank Diana Timmermans for her assistance throughout the last two years, her hard work is very much appreciated. I would also like to thank my fellow BME colleagues, Yara Hosein, Pencilla Lang, Brandon Miles, Paul Prowse, and Corey Smith for their assistance with the BME Student Committee.

I would like to thank all of my collaborators: Dr David O'Gorman and his technicians Yan Wu and Andrew Gould, Dr Kem Rogers and his technician Jessica Davies, Dr David Litchfield and Laszlo Gyenis, and Dr Eric Ball. I would also like to thank my past and present group members: Dr Karen Kennedy, Dr Donna Padavan, Dr Kenneth Wong, Elaine Wong, Suanne Mahabir, Marko Spaic, Darcy Small, Zachary Armstrong, Jennifer Redwood, Justin Cook, Sara Makaremi and Asha Parehk. Thank you for enduring my numerous questions and being patient with me. I would also like to thank my sources of funding: the Canadian Institute of Health Research, the Ontario government and the Advanced Food and Materials Network, without their assistance this work could not be completed.

I would also like to thank my friends and family for the constant support while I continue to pursue my goals and further my education. Special thanks goes to my sisters, Tiffany and Vanessa Lee, and my good friends Carly Beneteau, Brett Elsdon, Joshua Hwang, Benjamin Lee, Elliott Nguyen, Ea-Ling Seun, Adam Tasca, Zixi Wang and Yan Yeung. What would I do without Trivia Night's at the Grad Club? Thanks for all your support in everything I do.

Table of Contents

List of Figures

List of Tables

List of Appendices

List of Abbreviations

3D	Three Dimensional
AHV	Aortic Heart Valve
BSA	Bovine Serum Albumin
DDS	Drug Delivery System
ECM	Extracellular Matrix
ELISA	Enzyme-Linked Immunosorbant Assay
FITC	Fluorescein-isothiocyanate
FTIR	Fourier Transformed Infrared
GAGs	Glycosaminoglycans
HFIP	Hexafluoroisopropanol
LSCM	Laser Scanning Confocal Microscopy
PBS	Phosphate buffered Saline
PCL	Poly(ε-caprolactone)
PDGF	Platelet Derived Growth Factor
PEEP	Poly(ethyl ethylene phosphate)
PEG	Poly(ethylene-glycol)
PHB	Poly-4-hydroxybutyrate
PLGA	Poly(lactic-*co*-glycolic acid)
P(LDL)LA	Poly(L-lactide-co-D,L-lactide)
PLLA	Poly(L-lactic acid)
RACs	Radial Arterial Cells
SDS-PAGE	Sodium Dodecyl Sulfate Polyacrylamide Gel Electrophoresis
SEM	Scanning Electron Microscopy
TBS	Tris-base Buffered Saline
TC	Tropocollagen
TE	Tissue Engineering
TEM	Transmission Electron Microscopy
TFE	Trifluoroethanol
UV	Ultraviolet

Chapter 1: Introduction

Aortic heart valve replacements have been heavily studied over the past fifty years, and yet an ideal valve replacement still does not exist. An ideal valve replacement should be biocompatible, non-thrombogenic and offer continuous remodeling and repair to grow with the patient [1]. Tissue engineering provides a promising alternative for the development of tissue replacements; the key support structure used for tissue regeneration is the scaffold. A new form of biomaterials being developed are smart materials, which intuitively provide physical and biological cues necessary for tissue regeneration [2]. These smart materials often combine the design of a tissue structure coupled with the delivery of biologically active compounds.

One method for creating suitable scaffolds for tissue engineering is by electrospinning. Electrospinning creates continuous, non-woven nanofibrous 3D meshes with fibres in either a random or ordered orientation. Moreover, therapeutic proteins can be encapsulated within the polymer fibres via coaxial electrospinning. Many electrospun polymer fibres promote cell adhesion, yet cannot provide the necessary signals for cell proliferation, migration and differentiation, which is crucial for the success of a tissue engineered implant [3]. By incorporating therapeutic proteins called growth factors into the nanofibres, controlled release within the scaffold may be achieved, signalling essential cues for tissue development [2].

This work aims at the creation of a unique core-shell growth factor containing nanofibrous scaffold that is anticipated to provide optimal conditions to control and guide tissue formation. An understanding of growth factor delivery from the scaffold is important for developing systems that accurately reflect the growth factor concentrations in native tissue [4]. The scaffold will be considered in the design and fabrication of a tissue engineered heart valve replacement that promises to be a living implant with the ability to regenerate and grow with the patient.

The main focus of this work is to create a foundation for the development of a bioactive scaffold capable of localized drug delivery by encapsulating various therapeutic substances within core-shell nanofibres. This will be accomplished using coaxial electrospinning and the release kinetics will be examined.

The main objectives of this work are:

- To encapsulate proteins within core-shell nanofibres composed of Poly (ε-caprolactone) (PCL) via coaxial electrospinning
- To analyze the release of Bovine Serum Albumin (BSA) from core-shell PCL fibres using the Bradford Assay
- To develop a method to measure the release of Platelet Derived Growth Factor (PDGF) from PCL core-shell fibres using Enzyme Linked Immunosorbent Assay (ELISA)
- To analyze the biocompatibility of PCL core-shell scaffolds *in-vitro* using porcine Radial Artery Cells (RACs)
- To isolate and purify type I collagen from rat tails
- To electrospin solid and hollow fibres composed of type I collagen

Chapter 2: Background and Literature Review

2.1 The Aortic Heart Valve

2.1.1 Structure and Function

The heart is an organ used to circulate blood throughout the body. It is composed of four chambers that are connected by heart valves. These valves are used to maintain unidirectional blood flow through the heart during the cardiac cycle. The aortic heart valve (AHV) is a semi-lunar valve composed of three leaflets and is located between the left ventricle and the aorta.

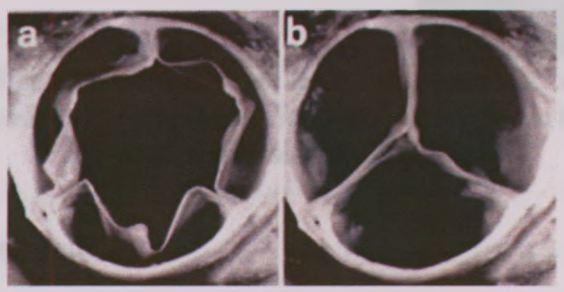

Figure 2.1: AHV leaflets during valve (a) opening and (b) closing. Reprinted with permission from [5].

The leaflets are flaps of connective tissue that create a seal, preventing regurgitation of blood back into the heart (Figure 2.1) [5]. The unique three layered structure of the leaflets allows them to withstand repetitive mechanical stresses over time. The layer facing the inside of the heart is called the ventricularis, and is composed of randomly orientated collagen fibres and radially aligned elastin fibres (Figure 2.2b). The abundance of elastin in the ventricularis is what gives the leaflet the ability to extend and recoil [5]. The spongiosa, the central layer, is a gelatinous lamina composed of glycosaminoglycans (GAGs). This layer contains a large amount of water and is responsible for absorbing and cushioning the compressive forces during the cardiac cycle [6]. Finally, the fibrosa faces the outside of the heart and is composed of circumferentially aligned, crimped collagen nanofibres (Figure 2.2a). This arrangement confers the valve its durable mechanical properties and acts as the load-bearing portion of the tissue [7].

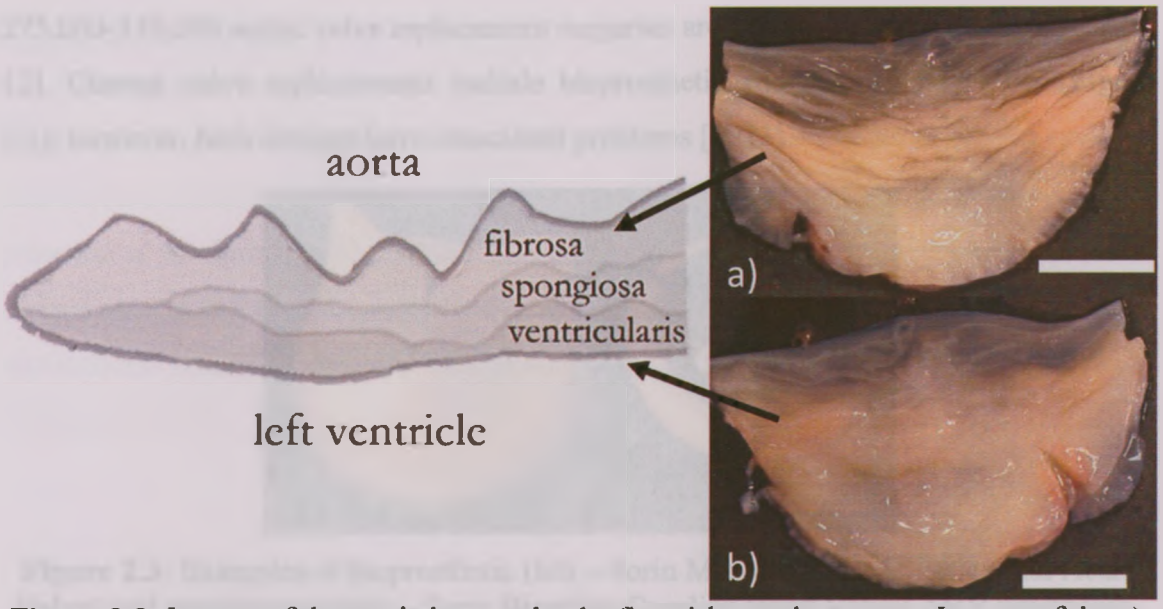

Figure 2.2: Images of the aortic heart valve leaflet tri-layered structure. Images of the a) fibrosa and b) ventricularis of a bovine aortic valve leaflet. Scale bar is 1 cm. (Reprinted with permission from [8]).

2.1.2 Disease and Treatment

Valvular heart disease continues to play a significant role in cardiovascular morbidity and mortality. The most prevalent forms of AHV disease include congenital AHV deformation, aortic stenosis and aortic regurgitation [9]. Congenital AHV disease is present in ~1% of the population and is characterized by a malformation of the valve resulting in a total or partial absence of one or more leaflets [5]. This in turn can cause stenosis, narrowing of the valve opening, and/or regurgitation, backflow of blood into the heart [10]. Aortic valve stenosis is a degenerative disease characterized by calcification and stiffening of leaflet tissue, and in effect it decreases the valve orifice area; aortic regurgitation is characterized by improper valve closing, which causes blood back flow into the heart [10-11].

Treatment of AHV disease includes valve repair or replacement; however, valve repair is not commonly recommended because of irreversible damage sustained by the valve and ineffective methods for supporting the damaged tissue [10]. Valve replacement is one of the most common surgical procedures with 87,000 heart valve replacement performed annually, accounting for 12% of all open heart procedures done in the U.S. (2000), and

275,000-370,000 aortic valve replacement surgeries are performed globally each year [9, 12]. Current valve replacements include bioprosthetic and mechanical valves (Figure 2.3); however, both designs have associated problems [1, 13].

Figure 2.3: Examples of bioprosthetic (left – Sorin Mitroflow Aortic Pericardial Heart Valve) and mechanical (right – Sorin Bicarbon Overline Heart Valve) AHV prostheses. Scale bar is 1 cm.

Mechanical valve replacements are generally made of pyrolytic carbon or metals coated with pyrolytic carbon, and are organized into folding discs anchored by hinges. This geometry creates several problems resulting in poor hemodynamics, platelet activation and thrombolytic complications [14]. As a result, patients are required to be on anticoagulants to avoid clot formation; however, this creates an additional risk of anti-coagulant induced haemorrhaging, which accounts for ~2 % of adverse events associated with AHV replacement [14].

Bioprosthetic valves are a viable substitute, but their use is limited due to poor long-term durability [15]. Current bioprosthetic valve designs include glutaraldehyde fixed decellularized porcine aortic heart valve or glutaraldehyde fixed bovine pericardium mounted onto a stent. Tissue valves are subject to higher rates of tissue degradation and calcification relative to mechanical or native valves, and it is thought to be caused by remaining cell debris and glutaraldehyde [15]. These designs unfortunately all have limited durability related to their acellular nature, calcification and their inability to repair, remodel or grow with the patient.

2.2 Electrospinning

2.2.1 Fundamentals

Electrospinning was first patented in 1934 by Formhals, and is a technique used to create non-woven, submicron fibres by extruding a polymer solution from a spinneret in the presence of an electric field [16]. Due to the simplicity and versatility of electrospinning, several natural and synthetic polymers have been successfully electrospun for a variety of applications including textiles, wound dressings, drug delivery and tissue engineering scaffolds [17-24].

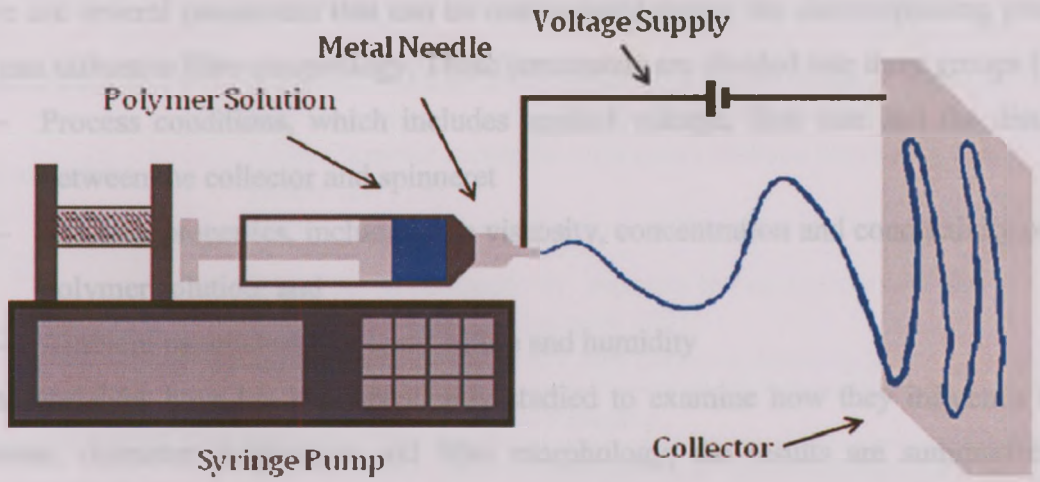

Figure 2.4: Typical electrospinning setup including syringe pump, syringe with metal needle, metal collecting plate and a power supply.

Electrospinning has been extensively studied and the general setup includes a syringe filled with polymer solution, metal needle, voltage supply, metal collector and syringe pump (Figure 2.4) [17-25, 27-34]. The polymer solution is extruded through the metal needle at a flow rate controlled by the syringe pump. The voltage supply is connected to the metal needle and grounded collecting plate and creates an electric field between them. As the polymer solution is extruded from the needle, the electric field induces charge along the surface of the droplet, creating a force opposite the surface tension [25]. As the charge density increases, the droplet becomes extended and forms a conical structure called the Taylor Cone (Figure 2.5) [26]. At a critical voltage, a single polymer jet is ejected from the cone surface and undergoes a series of whipping instabilities and, as the solvent evaporates, deposits non-woven nanofibres on the collector [27-28].

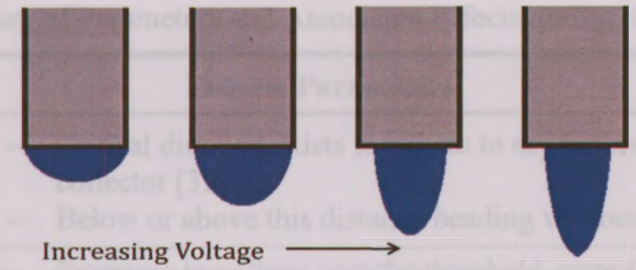

Figure 2.5: Polymer solution droplet at the needle tip developing into the Taylor cone under increasing electric field.

2.2.2 Parameters of Interest

There are several parameters that can be manipulated during the electrospinning process that can influence fibre morphology. These parameters are divided into three groups [19]:

- Process conditions, which includes applied voltage, flow rate and the distance between the collector and spinneret
- Solution properties, including the viscosity, concentration and conductivity of the polymer solution; and
- Ambient parameters like temperature and humidity

These variables have been independently studied to examine how they influence fibre diameter, diameter distribution and fibre morphology; the results are summarized in Table 2.1. An unfavourable morphology that can result during electrospinning is called beading, which occurs when the ejected polymer jet is still fluid and wet when it hits the collector [29]. Beading occurs because the charge on the surface of the jet dissipates, decreasing the elongation force, creating fibres have a "bead-on-string" appearance as seen in Figure 2.6 [30].

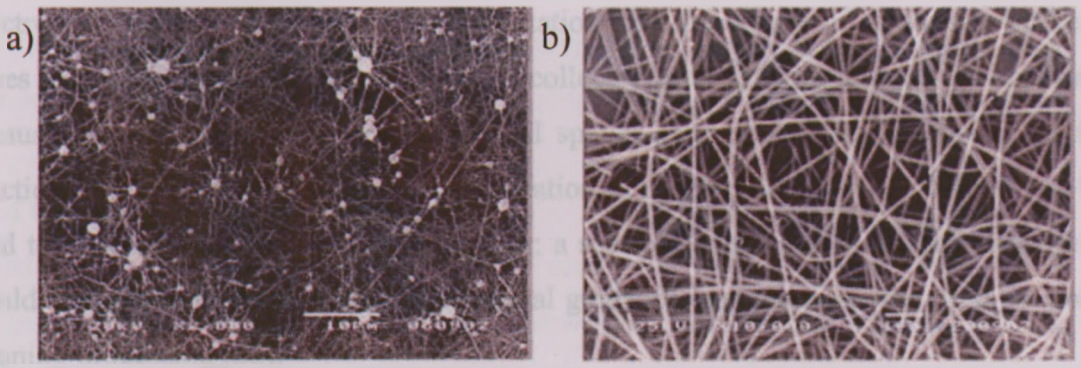

Figure 2.6: SEM images illustrating electrospun polyamide-6 fibres with (a) and without beading (b). Scale bar are 10 μm and 1 μm for a and b respectively. (Reproduced with permission from [31])

Table 2.1 – Summary of Parameters and Associated Effects during Electrospinning

Process Parameters	
Distance	– Critical distance exists for fibres to dry before they reach the collector [32] – Below or above this distance beading will occur [24]
Voltage	– Increases in voltage past the threshold cause the Taylor cone to dissipate into the needle causing beading [18] – Further increases cause splaying, which creates an ambiguous effect on the fibre diameter and diameter distribution [33]
Flow Rate	– Increased flow rates lead to larger diameters [33] – Low flow rates decrease beading and fibre diameter [24]
Solution Parameters	
Concentration	– Has the strongest influence on fibre diameter [24] – Fibre diameter increases with concentration according to a power law [18] – If the concentration is too low electrospraying will occur [31]
Conductivity	– Increases in conductivity, increase the charge density and as a result decrease fibre diameter [33] – Increases in conductivity also decrease beading [29]
Ambient Parameters	
Temperature	– Increased temperature decreases the fibre diameter [19] – Thought to be related to changes in viscosity [31]
Humidity	– Increased humidity leads to larger fibre diameters [19] – Increases in humidity can lead to pore formation on surface of fibres [34]

2.2.3 Fibre Orientation

Electrospinning is unique in that the orientation and the degree of alignment between fibres can be manipulated by the type of collector used [35]. Alignment is important because most native tissues have a defined spatial arrangement that is significant for function, like that of AHV leaflets. Incorporation of nanostructures onto scaffolds can be used to encourage and guide cell behaviour; a scaffold composed of aligned nanofibres would instinctively provide this informational guidance, and eliminate the need for post-spinning processing [36].

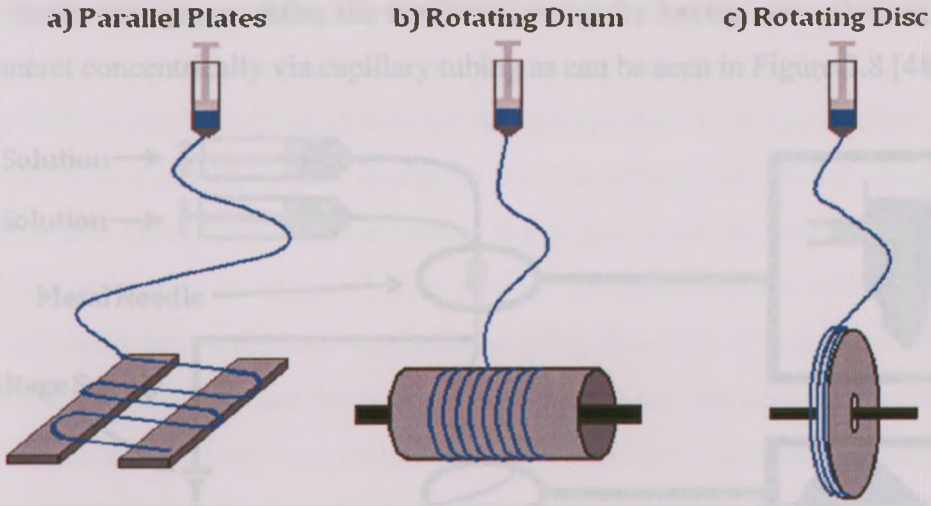

Figure 2.7: Different types of electrospinning collectors used to create aligned fibres.

There are currently three main types of collectors used to generate aligned fibres: parallel plates, rotating drums and rotating discs (Figure 2.7). Parallel plates are composed of two grounded conductive plates that capture aligned fibres between them; a drawback for this method is that the fibre length is limited to the distance between the plates [37-38]. The other two methods are a rotating drum or disc, where the speed of rotation influences the degree of alignment between fibres [39-40]. The collectors need to be moving fast enough to align the fibres, but not so fast that it breaks the fibres as they are being collected [41-42]. A rotating drum has benefits because they come in different shapes and sizes, which can influence fibre alignment and diameter, and provides a larger area for fibre collection [24]. Fibres can be collected on a rotating disc two ways: directly on the disc's edge with a yarn-like structure or on a glass cover slip attached to the disc's edge [43]. The development of new collectors has been investigated; for example, a study used a rotating wire mandrel to produce self-crimping nanofibres, which had similar structural and mechanical properties to that of native collagen fibrils, like in AHV leaflets [44].

2.2.4 Coaxial Electrospinning

Coaxial electrospinning creates hollow, or core-shell, nanofibres that can be used to encapsulate various substances. Core-shell nanofibres have applications in microfluidics, textiles and fabrics, and drug delivery [45-47, 21]. Initially proposed by Loscertales et al.,

coaxial electrospinning modifies the traditional set-up by having two solutions feed into one spinneret concentrically via capillary tubing as can be seen in Figure 2.8 [48].

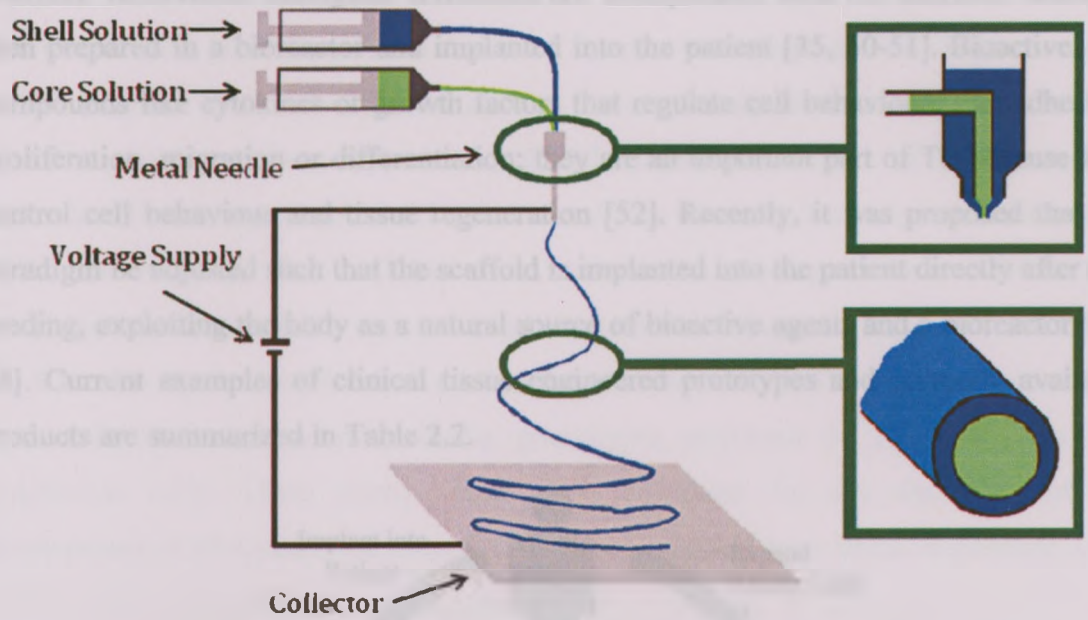

Figure 2.8: Schematic diagram of coaxial electrospinning setup illustrating the concentric spinneret and fibre structure (Adapted from [45]).

The parameters that influence fibre morphology during electrospinning have the same trend in coaxial electrospinning; however, there are new variables that need to be considered. In coaxial electrospinning the two solutions meet at the tip of the needle, and how they interact here can influence fibre structure. If the two solutions are immiscible a more defined core-shell structure can be produced; otherwise, mixing can occur and the core-shell structure is lost and beading occurs [45, 47]. Furthermore, the ratio of the core and shell solution flow rates can influence the ability to produce hollow fibres. It has been demonstrated that the optimal core-shell ratio should be between 1:3-1:6 [21, 49]. Ratios below this range do not provide enough shell polymer solution to encapsulate the core, and ratios above this range result in collapse of the hollow core [21].

2.3 Tissue Engineering

2.3.1 Principles

Tissue engineering (TE) is commonly understood to be an interdisciplinary field that uses a combination of engineering principles and life science to develop of *in vivo* tissue

substitutes that restore or improve tissue function [50]. The general concept, depicted in Figure 2.9, involves culturing patient cells from biopsy samples and seeding them onto a scaffold. Afterwards biological stimulants are incorporated with the scaffold, which is then prepared in a bioreactor and implanted into the patient [35, 50-51]. Bioactives are compounds like cytokines or growth factors that regulate cell behaviours like adhesion, proliferation, migration or differentiation; they are an important part of TE because they control cell behaviour and tissue regeneration [52]. Recently, it was proposed that the paradigm be adjusted such that the scaffold is implanted into the patient directly after cell seeding, exploiting the body as a natural source of bioactive agents and a bioreactor [53-54]. Current examples of clinical tissue engineered prototypes and currently available products are summarized in Table 2.2.

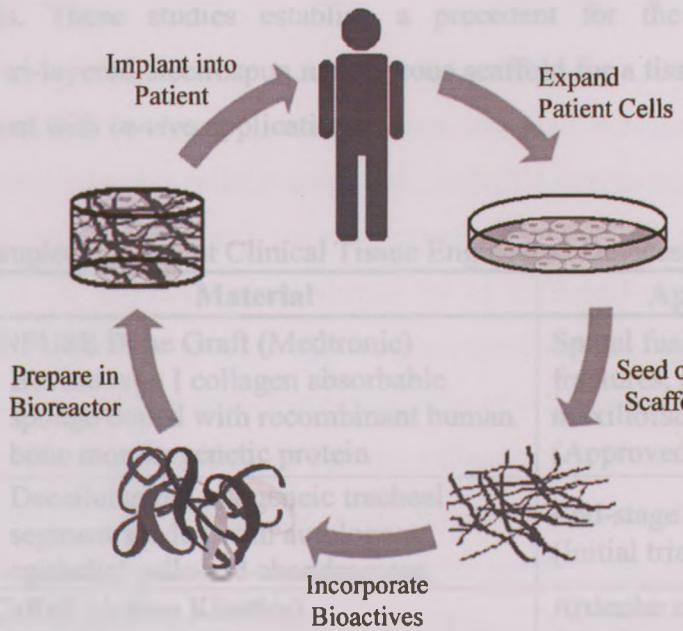

Figure 2.9: Schematic diagram illustrating the tissue engineering paradigm.

One of the first studies performed with a heart valve replacement composed of synthetic scaffolding was done by Hoerstrup et al. [55]. A tri-leaflet structure made of poly(glycolic acid) (PGA) coated with poly-4-hydroxybutyrate (PHB) was prepared via heat welding. The construct was conditioned in a bioreactor under pulsatile conditions for 14 days and implanted into sheep for up to 20 weeks. The valve replacements were functioning *in-vivo* and showed layered organization of collagen and GAGs; however, during the remodelling process the leaflets thickened, significant amounts of elastin were

not present and regurgitation occured after 16 weeks. Breuer et al. implanted a single tissue engineered valve leaflet composed of layered PGA and poly(lactic-*co*-glycolic acid) (PGLA) fibres, which were seeded with homologous myofibroblasts and endothelial cells [56]. They found that the TE valve leaflet had thickened but presented an ECM similar to that of native valve tissue. A recent study performed by Schmidt et al. created a poly(L-lactide-co-D,L-lactide) (P(LDL)LA) tri-leaflet mesh by thermal fixation and coated it with electrospun P(LDL)LA nanofibres to mimic the tri-layered structure of AHV leaflets [57]. The scaffolds were seeded with autologous bone marrow and peripheral blood stem cells, cultured in a bioreactor for 7 days and implanted into sheep for 4 weeks. Again leaflet tissue thickening occurred and elastin was not present, but stem cells had demonstrated similar phenotypic responses as myofibroblasts and endothelial cells. These studies establish a precedent for the feasibility of the development of tri-layered electrospun nanofibrous scaffold for a tissue engineered AHV leaflet replacement with *in-vivo* applications.

Table 2.2 – Examples of Current Clinical Tissue Engineered Devices and Prototypes

	Material	**Applications**
Bone [58]	INFUSE Bone Graft (Medtronic) - Bovine type I collagen absorbable sponge doped with recombinant human bone morphogenetic protein	Spinal fusion, tibial fractures, and oral maxillofacial bone grafting (Approved 2002)
Trachea [59]	- Decellularized allogeneic tracheal segment seeded with autologous epithelial cells and chondrocytes	End-stage airway disease (Initial trial)
Cartilage [60]	CaReS (Arthro Kinetics) - Rat tail type I collagen matrix seeded with autologous chondrocytes	Articular cartilage injury (Germany Approved in 2007)
Bladder [61]	- Composite scaffolds composed of collagen and PGA seeded with autologous urothelial and smooth muscle cells	End-stage bladder disease requiring cystoplasty (Initial stages)
Skin [62]	ICX-SKN (Intercytex) - Allogenic collagen matrix seeded with allogenic fibroblasts	Skin grafts (Phase II Clinical Trials)

2.3.3 Scaffolds for Tissue Engineering

One of the most critical components of TE is the scaffold: a 3D, artificial structure that supports cell growth and tissue development [35, 50, 54, 63]. The scaffold acts as an artificial extracellular matrix (ECM), which is the native fibrillar network composed of GAGs, proteoglycans and proteins used to support cell growth and influence cell behaviour [64]. Scaffold design is of particular importance because integration of the neo-tissue into the native tissue is crucial for success [65]. This implies that the scaffold has to be biodegradable such that the artificial implant will be completely replaced by newly formed tissue. Furthermore, the degradation rate of the scaffold should be controlled such that it closely matches that of matrix formation so that support is maintained during tissue development [3, 65].

There are significant characteristics to consider when designing a scaffold. It is important for scaffolds to have a high porosity with suitable pore size, contain nano-scale features and be capable of elucidating cellular responses. A highly porous scaffold allows for the efficient transfer of nutrients and wastes between the scaffold and its surrounding environment [35]. In additions pores should be of sufficient size to allow for cell migration throughout the 3D network. Electrospun nanofibres are highly porous and have a large surface area to volume ratio, increasing rates of cell adhesion and migration [66]. The dimensions and scale of a scaffold can also influence cell behaviour. Recently, there has been a focus on developing 3D scaffolds on the nanoscale because stronger interactions between the cells and scaffold, and the scaffold and host tissue have been demonstrated using smaller scale features [36, 54, 66].

Furthermore, the physical and mechanical properties of a scaffold should closely match those at the implant site such that it may tolerate the forces acting on it and the surrounding environment upon implantation. This is particularly important for AHV TE, where the implant will have to be able to withstand the various tensile and compressive forces accompanying pulsation, pressure gradients and blood flow [51, 66]. Furthermore, it has been demonstrated that cells can sense the stiffness of the material and respond

accordingly [67]. Therefore, material selection can be used to influence the scaffold properties and can effectively guide cell behaviour and cytoskeleton rearrangement [68].

The native ECM plays several roles in tissue development as a support structure for cell and tissue growth, and as a depot of growth factors and signalling molecules that are released from the matrix to regulate cell behaviour [65, 69]. Many electrospun synthetic biodegradable polymers promote cell adhesion, yet cannot provide the necessary biochemical signals to control and guide tissue regeneration [3, 63]. Recently, the concept of instructive materials has been popularized, where the material is loaded with information to properly guide gene expression, cell migration and differentiation, like the native ECM [63-64]. This can be achieved through a variety of methods including manipulation of the scaffolds mechanical properties, surface functionalization with bioactive molecules (like RGD peptides), incorporation of matricellular components (collagen, laminin etc.) or controlled release of signalling molecules from the scaffold [3, 36, 53, 54, 65, 67]. Electrospun nanofibrous meshes are a promising choice for TE scaffolds because they fulfill most of these structural, physical and biological requirements.

2.4 Controlled Release

2.4.1 Drug Delivery Systems

Controlled drug delivery systems (DDS) are designed to release therapeutic substances at a predetermined rate. Controlled delivery offers several important advantages over conventional drug therapies in terms of drug administration, biodistribution and safety [70]. Controlled DDS help maintain the drug concentration in the therapeutic range, which exists between the toxic level and the minimum effective level (Figure 2.10). Also, controlled release improves regulation of drug dosage resulting in higher patient compliancy and less side effects [71].

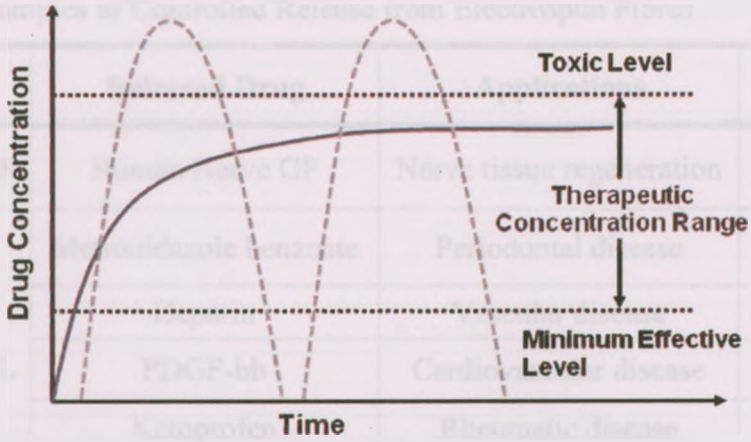

Figure 2.10: Drug release profiles comparing conventional multiple dose therapy (dashed line) with sustained release profile (solid line).

DDS can protect biologically sensitive molecules and thus preserve medications that are rapidly destroyed by the body, increasing bioavailability at the target site. Furthermore, controlled drug delivery offer localized delivery of the drug to a specific portion of the body, decreasing systemic side effects [72]. Some examples of polymeric DDS include diffusion based systems (reservoirs and matrices), erosion or chemical controlled systems (degradation or bond-cleavage) and solvent activated systems (hydrogels) [70-71].

Electrospun nanofibres are currently being investigated as controlled release DDS (Table 2.3) for applications in gene therapy, antibiotic wound dressings and TE [73, 65, 21, 22, 74]. There are two methods in which therapeutic substances can be incorporated into electrospun polymer fibres: blending or coaxial electrospinning. Blend electrospinning involves mixing the polymer and the drug into one solution that is then spun into one solid fibre. Blending exposes the drug to harsh solvents, which can greatly decrease its bioactivity. Additionally, blend electrospinning is expected to provide less control of the release process as the drugs will be distributed randomly throughout the cross-section of the fibre. Conversely, coaxial electrospinning has been demonstrated to have tuneable release kinetics, allowing for regulation of the release kinetics [49]. Furthermore, coaxial electrospinning can preserve the biological activity of drugs due to mild reaction conditions [21]. Thus sensitive bioactive therapeutics, like growth factors, can be successfully incorporated and released from nanofibrous scaffolds without a significant loss in activity.

Table 2.3 – Examples of Controlled Release from Electrospun Fibres

Shell Polymer*	Released Drug	Applications	References
PCL-PEEP	Human Nerve GF	Nerve tissue regeneration	[75]
PCL	Metronidazole benzoate	Periodontal disease	[76]
	Heparin	Vascular disease	[77]
	PDGF-bb	Cardiovascular disease	[49]
	Ketoprofen	Rheumatic disease	[22]
	Plasmid DNA	RNA interfere	[73]
PLLA	Paclitaxel	Antitumor agent	[74]
PLGA	Basic Fibroblast GF	Ligament/tendon regeneration	[78]
	Cefazolin	Wound healing	[79]

*PLLA - Poly(L-lactic acid), PCL-PEEP – PCL-co- Poly(ethyl ethylene phosphate)

2.4.2 Release Kinetics

The most common empirical model used to illustrate drug release is the Power Law developed by Ritger and Peppas (Eq. 2.1) [80]:

$$\frac{M_t}{M_\infty} = kt^n \tag{2.1}$$

Where M_t is the amount of drug released at time t, M_∞ is the total amount of drug loaded, n is the diffusional exponent and k is a constant that accounts for characteristics relating to the geometry of the device as defined by Ritger and Peppas [80]. The value of the diffusional exponent n is indicative of the transport mechanism the system is exhibiting (Table 2.4). The Power Law can be viewed as a simplification of overlapping mechanisms of drug transport: Fickian diffusion and Zero-order kinetics.

Table 2.4 – Power Law Variables n and k Defined in Relationship to Geometry [80]

	Diffusion Exponent, n		
Geometry	*Thin Slab*	*Cylinder*	*Sphere*
Diffusion	0.50	0.45	0.43
Anomalous	$0.50 < n < 1.0$	$0.45 < n < 1.0$	$0.43 < n < 1.0$
Zero Order	1.0	1.0	1.0
	Kinetic Constant, k		
	$4(D/\pi l^2)^{1/2}$	$4(D/\pi a^2)^{1/2}$	$6(D/\pi a^2)^{1/2}$

*l is the thickness of the slab and a is the radius of the cylinder/sphere

Most controlled release systems are based on diffusion, the migration of a drug from one point to another, and can be either reservoir or matrix based systems. Reservoir systems encapsulate the drug within a polymer layer and are governed by Fick's First Law of Diffusion (Eq. 2.2) [71]:

$$J = -D\frac{\delta C}{\delta x} \tag{2.2}$$

Where J is the flux, dC/dx is concentration gradient and D is diffusion coefficient. The release rate is determined by the ability of the drug to diffuse through the polymer coating and is independent of the initial drug concentration and time. Drug release from reservoirs is mainly influenced by the thickness of the outer polymer layer and the diffusion coefficient, so it follows zero-order kinetics [81].

Matrix DDS have the drug dissolved or dispersed within the polymer matrix. Although the rate determining step is diffusion through the polymer, matrix systems are dependent on the initial concentration of the drug, C_0, and the drug's solubility, C_S. In dissolved systems ($C_0 < C_S$), the release rate decreases with time and follows Fick's Second Law of Diffusion (Eq. 2.3):

$$\frac{\delta c}{\delta t} = D\frac{\delta^2 C}{\delta x^2} \tag{2.3}$$

Where C is the concentration, D is the diffusion coefficient and x is the one dimensional direction of diffusion. This has been adapted by Ritger and Peppas for geometries of thin slabs (Eq. 2.4a, Eq. 2.4b) and cylinders (Eq. 2.5) [80]:

When:

$$0 < \frac{M_t}{M_\infty} < 0.6 \qquad \frac{M_t}{M_\infty} = 4\left(\frac{Dt}{\pi l^2}\right)^{1/2} \tag{2.4a}$$

When:

$$0.4 < \frac{M_t}{M_\infty} < 1.0 \qquad \frac{M_t}{M_\infty} = 1 - \frac{8}{\pi^2}\, exp\left(\frac{-\pi^2 Dt}{l^2}\right) \tag{2.4b}$$

When:

$$0 < \frac{M_t}{M_\infty} < 0.2 \qquad \frac{M_t}{M_\infty} = 4\left(\frac{Dt}{\pi a^2}\right)^{1/2} - \frac{Dt}{a^2} \tag{2.5}$$

Where M_t is the amount of drug released at time t, M_∞ is the total amount of drug loaded, D is the diffusion coefficient, l is the thickness of the slab and a is the radius of the cylinder. In dispersed systems ($C_0 > C_S$), the rate is limited by the ability of the drug to dissolve in the matrix. This type of release has been modelled by Higuchi (Eq. 2.6) [82]:

$$\frac{M_t}{A} = \sqrt{D(2c_0 - c_S)c_S t} \tag{2.6}$$

Where M_t is the cumulative amount of drug released at time t, A is the surface area, D is the diffusion coefficient, C_0 is the initial drug concentration, and C_S is the solubility of drug in polymer. This model makes several assumptions [71, 82]: (i) that $C_0 >> C_S$, (ii) swelling is negligible, (iii) perfect sink conditions are maintained, (iv) constant drug diffusivity, and (v) one-dimensional diffusion only, i.e. edge effects are negligible.

Drug delivery from matrix systems depends on the solubility of the drug in the polymer; this becomes a problem in cases involving water-soluble drugs (like proteins) with hydrophobic polymers. In these cases, the drugs are dispersed throughout the polymer and can only dissolve when system is placed in an aqueous media. Drugs do not diffuse through the polymer, rather they are released through the matrix's water-filled pores [81].

2.5 Material Selection

2.5.1 Polymers

2.5.1.1 Poly(caprolactone)

Poly(caprolactone) (PCL) is biocompatible, biodegradable polyester, and is prepared by polymerization via ring opening of ε-caprolactone as can be seen in Figure 2.11.

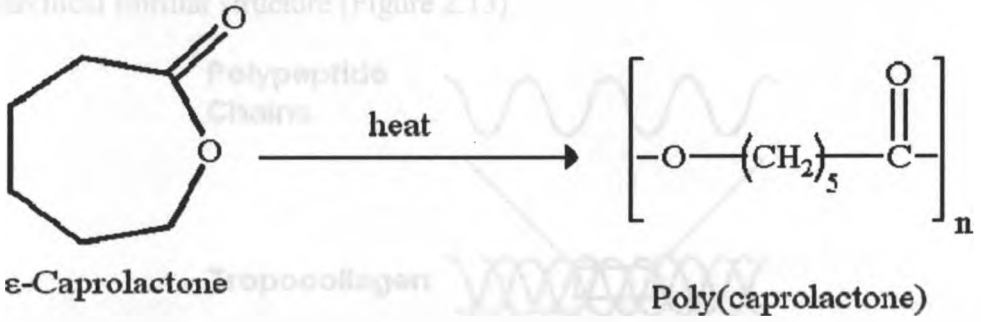

Figure 2.11: Reaction mechanism illustrating ring opening polymerization of ε-caprolactone into linear poly(caprolactone).

PCL can be degraded under physiological conditions through hydrolysis of its ester linkages, and because of this property, it is an attractive material for various uses biomedical applications. Currently there are several FDA-approved medical implants with PCL components, including medical sutures, drug delivery devices and implant coatings [83]. Furthermore, unlike other common biodegradable polymers, when PCL degrades its by-products are neutral and do not cause a change in the pH of the local environment [54].

2.5.1.2 Poly(ethylene glycol)

Poly(ethylene glycol) (PEG) is a flexible, water-soluble polyether that has a low toxicity and is used in a variety of medical applications (Figure 2.12). PEG has been demonstrated to act as a porogen when incorporated into the polymer matrix of DDS, and has the ability to modulate the release kinetics [84-85].

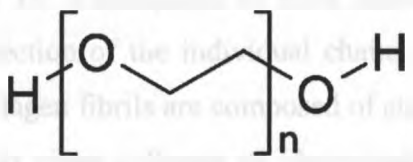

Figure 2.12: Chemical structure of poly(ethylene glycol).

2.5.1.3 Type I Collagen

Collagen is the most abundant protein in the body, with superior properties in terms of mechanical strength, thermal stability and wound healing [86]. It is a major component of skin, bone and muscle tissues, and several diseases have been linked to improper collagen production [87]. The unique physical properties associated with collagen are correlated to its hierarchical fibrillar structure (Figure 2.13).

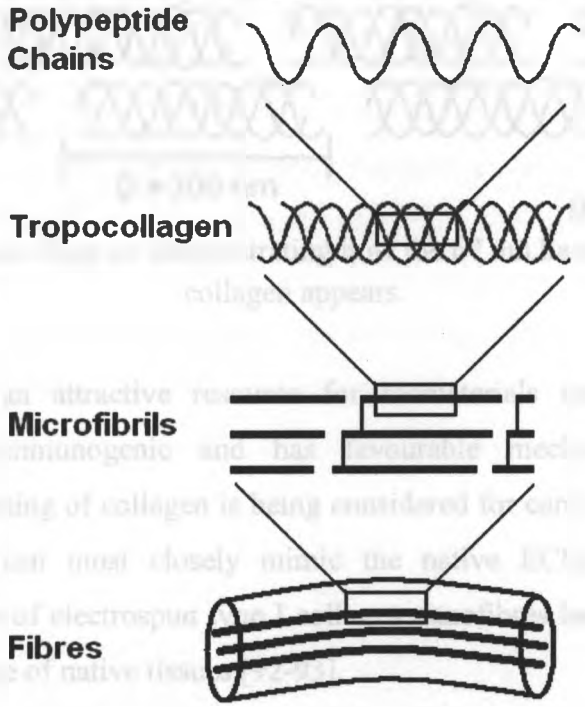

Figure 2.13: Schematic diagram illustrating collagen's hierarchical structure (Adapted from [88]).

Type I collagen is composed to two α_1 and one α_2 left-handed coiled polypeptide chains with the characteristic "Gly-X-Y" amino acid sequence. Glycine accounts for a third of all amino acid residues in collagen, and the X and Y residues are random amino acids but most commonly are proline or hydroxyproline residues [89]. These three polypeptide chains combine to create a single tropocollagen (TC) molecule, with a length of approximately 300 nm [88]. TC is composed of three chains coiled into a right-handed coil, opposite the native direction of the individual chains, and has a tertiary structure called a coiled-coil [86]. Collagen fibrils are composed of staggered TC groups with gaps approximately 67 nm, which gives collagen its characteristic banding pattern (Figure 2.14). Recently, one group was able to electrospin human placental collagen nanofibres

that exhibited the typical 67 nm banding pattern [90]. The larger collagen fibrils are held together by both intra and inter-strand hydrogen bonding and by strand-strand crosslinking. Finally, the collagen micro-fibrils join together to create larger structures in various bone, muscle and skin tissues [86].

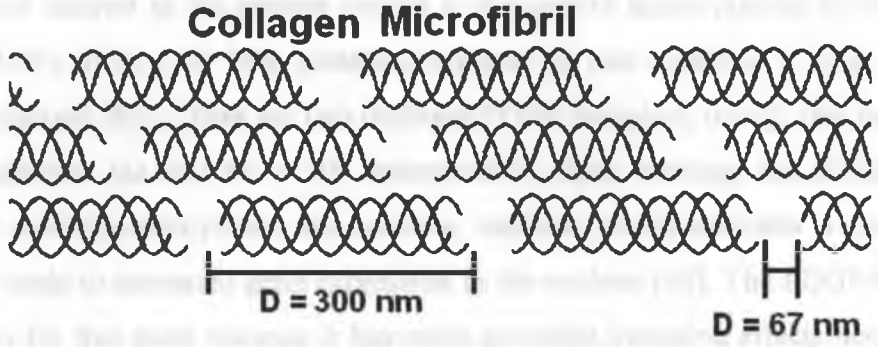

Figure 2.14: Schematic diagram demonstrating how the 67 nm banding pattern on native collagen appears.

Collagen has been an attractive resource for biomaterials research because it is biocompatible, non-immunogenic and has favourable mechanical properties. In particular, electrospinning of collagen is being considered for cardiovascular TE because the resulting fibres can most closely mimic the native ECM [91]. Recently, the mechanical properties of electrospun type I collagen nanofibres has been explored, with results within the range of native tissues [92-93].

2.5.2 Growth Factors

Growth factors are a class of polypeptides that influence cell behaviours like locomotion, proliferation and differentiation [2, 52, 94, 95]. The effects are often concentration gradient dependent; for example cell migration is induced in the direction of the concentration gradient [64]. Incorporation of growth factors is critical to the success of tissue engineered constructs because they can direct tissue development and remodelling [96]. Unfortunately, growth factors have a short lifetime *in-vivo* so controlled release of these substances would be ideal for sustaining long-term stimulation [2, 4]. Furthermore, growth factors improve communication between the cells, artificial matrix and surrounding environment, providing necessary signals for the integration of developing tissue [4, 96]. Some examples of growth factors used in current TE initiatives are

transforming growth factor beta, fibroblast growth factor, insulin-like growth factor and platelet derived growth factor [2, 94, 96].

2.5.2.1 Platelet Derived Growth Factor (PDGF)

Of particular interest to the present project is the growth factor platelet derived growth factor (PDGF). It is a 30 kDa protein composed of two subunits, a or b, joined by disulfide linkages [97]. There are two different PDGF receptors, α or β, that respond to a specific isoforms (aa and bb or ab respectively). Upon binding, the PDGF receptor undergoes auto-phosphorylation on tyrosine residues which activates a cascade that ultimately leads to increased gene expression in the nucleus [98]. The PDGF-bb isoform was chosen for this work because it has more powerful inductive effects because of its ability to active both α and β receptors [99]. PDGF-bb plays various roles in wound healing, tissue regeneration and tissue repair by recruiting cells and encouraging them to proliferate inside the wound [97, 99]. Furthermore, when cells are exposed to a PDGF concentration gradient, it induces them to migrate down the gradient [100].

Chapter 3: Materials and Methods

3.1 Materials

The following were purchased from Sigma Aldrich, Oakville, ON, Canada:

- Poly (ε-Caprolactone) (PCL) (440744, Molecular Weight of 80 kDa)
- Trifluoroethanol (TFE) (T63002, 2,2,2-TFE Reagent Plus®)
- Type I Collagen (C7661, Collagen, Type I; from Rat Tail)
- Hexafluoroisopropanol (HFIP) (105228, 1,1,1,3,3,3-hexafluoroisopropanol)
- Bovine Serum Albumin–Fluorescein Isothiocyanate (A9771, BSA-FITC)
- Poly (Ethylene Glycol) (309028, 10 kDa)
- Sodium Phosphate Dibasic Heptahydrate (431478, $Na_2HPO_4 \cdot 7H_2O$)
- Tween® 20 (93773, Tween® 20)
- Potassium Chloride (P9333, KCl)
- Glycine (241261)
- Sodium Dodecyl Sulphate (L4390, SDS)
- Ponceau S (P3504)
- Tris(hydroxymethyl)aminomethane (T1503, TRIS Base)
- Medium M199 (M4530)
- Formalin solution, neutral buffered, 10% (HT501128)

The following were purchased from R&D Systems, Minneapolis, MN, USA:

- Recombinant Human PDGF-BB (220-BB, > 97%)
- Human PDGF-BB DuoSet ELISA Development kit (DY220)
- ELISA Substrate Reagent Pack (DY999)

The following were purchased from Caledon Laboratories, Georgetown, ON, Canada:

- Sodium Chloride (7560-1, NaCl)
- Potassium Phosphate Monobasic (6660-1, > 99%)
- Ethanol (1500-1, > 95%)
- Sulphuric Acid (8825-1, > 95%)
- Acetic Acid (100-8-60, > 99%)

The following were purchased from Bio-Rad Laboratories (Canada) Ltd, Mississauga, ON, Canada:

- Protein Assay Dye Reagent Concentrate (500-0006)
- 30% Acrylamide/Bis Solution (161-0154)
- Tetramethylethylenediamine (TEMED) (161-0801)
- Ammonium Persulfate (APS) (161-0700)
- Bromophenol Blue (161-0404)
- Sodium Dodecyl Sulfate (SDS) (161-0301)
- Thick Blot Paper (170-3966)

The following were purchased from Invitrogen Canada Inc, Burlington, ON, Canada:

- Albumin From Bovine Serum, Alexa Fluor® 594 conjugate (Cat# A13101)
- Protein Assay Dye Reagent Concentrate (500-0006)
- Novex® Sharp Pre-stained Protein Standard (LC5800)
- Hoechst 33342 (H1399)
- Hanks' Balanced Salt Solution (HBSS, 14175-103)
- Dulbecco's Modified Eagle Medium (DMEM, 31053-028)
- Fetal Bovine Serum (FBS, 10091-155)
- Penicillin-Streptomycin (P/S, 15140-163)
- Amphotericin B (Fungizone®, 15290-018)

Additional Reagents:

- Fisher Bioreagents Bovine Serum Albumin (BSA) (Fisher Scientific Company, Ottawa, ON, Canada, Cat# BP1605100)
- Donkey Anti-Goat IgG- Horseradish Peroxidase Conjugated Secondary Antibody (Santa Cruz Biotechnology Inc., Santa Cruz, CA. Cat # SC-2033)
- Goat Anti-Rat Type I Collagen Alpha 1 Primary Antibody (Santa Cruz Biotechnology Inc., Santa Cruz, CA. Cat # SC-25974)
- Thermo Scientific Pierce SuperSignal West Pico Chemiluminescent Substrate (Fisher Scientific Company, Ottawa, ON, Canada, Cat# PI-34076)
- (BSA) (Fisher Scientific Company, Ottawa, ON, Canada, Cat# 9048-46-8)

- VECTASHIELD® Mounting Medium (Vector Laboratories Inc, Burlingame, CA, United States. Cat# H-1000)
- Complete, Mini, EDTA-free Protease Inhibitor Cocktail Tablets (Roche Diagnostics Canada, Laval, Quebec. Cat#11836170001)
- Instant Powdered Milk, Carnation brand

3.2 Solutions

3.2.1 Polymer Shell Solutions

Shell solutions of 12 wt% PCL and 5 wt% type I collagen were prepared as follows. PCL solutions were made by dissolving 1.2 g of PCL in 10 mL of TFE for 6 hours at room temperature. Type I collagen solutions were prepared by adding 94.2 mg of type I collagen from rat tail to 1 mL of HFIP, and vortexing to dissolve the collagen.

3.2.2 Protein Core Solutions

3.2.2.1 Bovine Serum Albumin

Previous work demonstrated that core solutions with BSA concentrations of 10 mg/mL were optimal for controlled release experiments [101]. In brief, 100 mg of BSA was dissolved in 10 mL of double distilled water and mixed thoroughly, to obtain a final concentration of 10 mg/mL. PEG, molecular weight of 10 kDa, was added to the core solution to provide stability and prevent mixing during the electrospinning process. PEG was dissolved into the BSA core solution to yield a final concentration of 200 mg/mL.

In addition, fluorescently labelled albumin proteins were used in core solutions for both PCL and type I collagen fibres for confocal imaging. For PCL and type I collagen fibres, BSA-FITC (ex. 495 nm, em. 520 nm) and BSA-Alexa Fluor 594 (ex. 590 nm, em. 620 nm) were used respectively. For these experiments, BSA concentrations of 10 μg/mL were determined to be optimal. For PCL scaffolds, BSA-FITC was dissolved in 1 mL of double distilled water and mixed thoroughly, to obtain a final concentration of 10 μg/mL. PEG was dissolved into the BSA core solution to yield a final concentration of 200 mg/mL. For collagen samples, PEG was dissolved into 80-90 % ethanol to yield a final concentration of 200 mg/mL. Next, BSA-FITC or BSA-Alexa Fluor 594 was slowly

dissolved in 1 mL of the PEG-ethanol solution, to obtain a final concentration of 10 µg/mL. Solutions were wrapped in tin foil and stored at 4 °C to preserve fluorescence.

3.2.2.2 Growth Factor Solutions

Recombinant human PDGF-bb was reconstituted using 4 mM hydrochloric acid containing 0.1 % BSA. Once fully dissolved, the solution was diluted with PBS containing 1 % BSA to yield a final concentration of 10-1000 µg/mL. Finally, PEG was added to this final solution at a concentration at 120 mg/mL

3.2.3 Buffers and ELISA Solutions

All buffers and solutions were prepared according to protocols found in Appendix A.

3.3 Methods

3.3.1 Electrospinning Setup

3.3.1.1 Single Pump

A single syringe pump (KD Scientific Inc.) was used to create solid PCL and collagen fibres. An electric field of 10 – 25 kV was created by connecting a voltage source (Glassman High Voltage Inc.) to the tip of the metal 30 gauge needle and a custom designed stationary metal collector, as shown in Figure 3.1.

Figure 3.1: Custom designed electrospinning setup.

3.3.1.2 Coaxial Electrospinning

Coaxial electrospinning was performed as previously established [101]. Two solutions were fed concentrically into a single metal needle tip using a capillary tube system. A flexible silica capillary tube, inner diameter of 250 μm, was threaded into the plastic syringe into a 20-gauge needle until it was flush with the metallic needle tip. The flow rates of each solution were independently controlled using a dual syringe pump (Model 33, Harvard Apparatus). The voltage source and metal collector were the same as those mentioned previously.

3.3.1.3 Parameters

Systematic trial and error was used to establish a standard set of variables which were able to form continuous fibres for both solid and hollow fibres. The combinations of variables that were used to create fibres are summarized in Table 3.1.

Table 3.1 – Electrospinning Parameters for Solid and Hollow Fibres

	Sample	Flow Rates* (ml/hr)	Distance (cm)	Voltage (kV)
Solid	12 wt% PCL	0.1-0.3	15-18	13-15
	5 wt% Collagen	0.15-0.25	18-20	10-12
Core-Shell	12 wt% PCL 10 μg/ml BSA-FITC + 20 wt% PEG	OFR: 0.30 IFR: 0.10	15-18	12-15
	12 wt% PCL 10 mg/ml BSA + 20 wt% PEG	OFR: 0.30 IFR: 0.10	15-18	13-15
	12 wt% PCL 1 mg/ml PDGF + 20 wt% PEG	OFR: 0.30 IFR: 0.08	15-18	13-15
	5 wt% Collagen 10 μg/ml BSA-FITC/Alexa Fluor 594 + 20 wt% PEG	OFR: 0.18 IFR: 0.06	18-20	9-11

*OFR is the outer flow rate of the polymer shell and IFR is the inner flow rate of the core solution

3.3.2 Isolation of Type I Collagen from Rat Tails

The procedure for the isolation of type I collagen from rat tails is detailed in Appendix B. In brief, frozen rat tails were thawed in 70% ethanol, dissected to expose the white

collagen fibres, which are then removed and placed in a separate sterile dish. Fibres are washed in 70% ethanol for 30 minutes, dried in a sterile Petri dish and left overnight to be sterilized under UV light. Collagen fibres are then dissolved in an acetic acid solution (1 mL of concentrated acetic acid in 1 L of distilled water) in cold room (at 4 °C) over 4-7 days. The solution is centrifuged at 11, 000 rpm (10, 000 g) for 2 hours and the supernatant was collected. Protein concentration was measured using the Sircol Collagen Assay and found to be 1.8 mg/ml. Collagen solution was stored at this point at 4 °C or frozen overnight at -20 °C and lyophilized for 1-2 days to obtain dry collagen powder.

3.3.3 Isolation of Porcine Radial Artery Cells

RAC isolation was performed as previously described and is detailed in Appendix C [102]. In brief, radial arteries were dissected out of porcine forelimbs in sterile lab conditions. The porcine radial arteries were minced and digested in a 0.08% collagenase, 0.25μg/mL Amphotericin B, and 1% Penicillin/Streptomycin solution for 24 hours at 37°C with constant stirring. The solution was then centrifuged for 5 minutes at 1100 rpm and the supernatant was discarded. Tissue pieces from the pellet were plated onto 100-mm^2 dishes and cells were removed after substantial cellular outgrowth.

3.4 Characterization

3.4.1 Microscopy

3.4.1.1 Scanning Electron Microscopy (SEM)

A Leo 1530 scanning electron microscope was used to obtain images of solid fibres. An accelerating voltage of 2 kV was used because it was a sufficient amount to prevent damage to the samples while still generating high resolution images. The surface morphology, diameter and diameter distribution were characterized using SEM images.

3.4.1.2 Transmission Electron Microscopy (TEM)

A Philips CM 10 transmission electron microscope was used to obtain images of core-shell collagen fibres. Collagen core-shell fibres were spun directly onto a TEM grid and an accelerating voltage of 2 kV was used. The core and fibre diameters and diameter distribution were characterized using TEM images.

3.4.1.3 Laser Scanning Confocal Microscopy (LSCM)

A Carl Zeiss Laser Scanning Confocal Microscope (LSM-410) equipped with an Argon/He/Ne laser and a Zeiss LSM 510 inverted microscope was used to image cell proliferation and encapsulated fluorescent proteins. DNA binding fluorescent dye Hoescht 33342 has excitation and emission wavelengths of 350 nm and 461 nm, respectively. The excitation and emission wavelengths of BSA-FITC are 488nm and 568nm, and Alexa Fluor 594 are 590 nm and 622 nm, respectively.

3.4.2 *In-vitro* Protein Release

3.4.2.1 Theoretical Loading Calculations

To determine the theoretical amount of protein loaded into the scaffolds, a mass balance approach was used; for detailed calculations see Appendix D. The ratio of the expected masses was used to determine what percentage of the scaffold mass could be attributed to the various components (like PCL, PEG, BSA, etc.).

3.4.2.2 Bradford Assay

The Bradford Assay developed by Bradford was used to measure protein concentration and the standard protocol is detailed in Appendix E [103]. In brief, the absorbance of Coomassie Brilliant Blue dye at 595 nm can be related to protein concentration according to Beer's Law. A Tecan Infinite® 200 PRO multimode reader was used to measure the absorbance at 595 nm.

3.4.2.3 ELISA

A sandwich ELISA was performed using Elisa DuoSet Development kits purchased from R&D Systems. The detailed protocol is located in Appendix F. Briefly a 96-well plate is coated with the primary detection agent over night, blocked with BSA then incubated with serially diluted samples for 2 hours. After rinsing, samples were incubated with a secondary antibody conjugated with horseradish peroxidase. Finally the samples are incubated with a 50:50 mixture of hydrogen peroxide and 3,3',5,5'-Tetramethylbenzidine for 20 minutes. The reaction is stopped with 2 N sulphuric acid and the absorbance is measured at 450 nm and 570 nm using a Tecan Infinite® 200 PRO multimode reader.

3.4.2.4 Protocol

Protein release was evaluated using core-shell scaffolds that were approximately 1 cm^2, incubated in phosphate buffered saline (PBS) at 37 °C for 10 days. Samples were submerged in 500 µL of PBS that was collected at various time points and replaced with fresh PBS kept at 37 °C. Samples were analyzed immediately or stored at 4 °C.

3.4.3 Cell Staining and Counting

Porcine RACs were used to measure cell viability on the PCL core-shell scaffolds. RACs were used because they have been established to be a viable surrogate cell source for aortic valve tissue regeneration [104]. Fibres were electrospun directly onto silicon wafers cut into 0.5 cm^2 squares, 15 000 cells were seeded and cultured for 24, 48 and 72 hours. At each time point, samples were fixed in a 10 % formalin solution for 30 minutes and mounted using a 1:100 mixture of Hoescht 33342 dye and Vectashield mounting media. Cell nuclei were visualized using LSCM.

3.4.4 Collagen Purification

3.4.4.1 Infrared Spectroscopy

Infrared data was collected using a Bruker Vector 22 Fourier Transformed Infrared (FTIR) spectrometer plus an Attenuated Total Reflectance (ATR) attachment (Pike Technologies Inc., Madison, WI) with a diamond crystal. Spectra were obtained in transmittance mode with 32 scans with a resolution of 4 cm^{-1}.

3.4.4.2 SDS-PAGE and Western Blotting

The detailed protocols are located in Appendix G. In brief, 500 µg of Type I Collagen from Rat Tail from Sigma-Aldrich (C7661) and our isolated samples were dissolved in 400 µl lysis buffer. Samples were homogenized with tissue homogenizer (Ultra Turrax T25 homogenizer, IKA Laboratory Equipment) for 2-3 minutes each and then sonicated on ice (Model 500 Dismembrator, Fisher Scientific) for 20 seconds total (in pulses of 5 seconds on 2 seconds off) at 30% amplitude. Finally, samples were heated to 95 °C for 3 minutes to solubilise collagen.

Samples, along with Novex® Sharp Pre-stained Protein Standard, were loaded into a 6% acrylamide gel and run at 120 V for 90 minutes. The samples were then transferred to a nitrocellulose membrane at 75 V for 90 minutes. The blot was incubated with the primary antibody Goat Anti-Rat Type I Collagen Alpha 1 for 1 hour. After three washes, it was incubated for 1 hour with the secondary antibody Donkey Anti-Goat IgG- Horseradish Peroxidase Conjugated. Finally, the blot was incubated for 5 minutes with Super Signal and imaged using a ChemiGenius 2 BioImaging System from Syngene.

3.5 Statistics and Data Analysis

Statistical analysis was carried out using Microsoft Excel (Microsoft Corp.) or Sigma Plot (Systat Software Inc). Data was analyzed by one-way analysis of variance (ANOVA) or student's t-test to determine significance between groups. In all experiments p-values of less than 0.05 were considered significant.

Chapter 4: Results and Discussion

The main objective of this work is to create core-shell nanofibres composed of type I collagen with encapsulated growth factors, which can be used as a scaffold for heart valve leaflet tissue regeneration. In order to achieve this goal, a well-established biocompatible and biodegradable polymer, PCL, is used for the development of a method for creating core-shell nanofibres. It is important to have this foundation such that a detailed understanding of the coaxial electrospinning process and the mechanisms of release from hollow fibres can be well understood. The incorporation of a model protein, BSA, into the core of the PCL fibres is utilized to study and comprehend the underlying release kinetics. Afterwards, PDGF can be incorporated into the PCL model fibre system to evaluate its release. The BSA and PDGF containing scaffolds can have their *in-vitro* performance compared to demonstrate successful release from the core and preservation of PDGF activity. Finally, core-shell fibres consisting of type I collagen as the polymer shell and BSA and PDGF in the core can be prepared and their release kinetics studied for use as scaffold materials for heart valve leaflet tissue regeneration.

4.1 Preparation of Core-shell PCL/BSA Fibres

The initial portion of this work involved learning how to create core-shell nanofibres via coaxial electrospinning. Preliminary parameters were: 12 wt% PCL polymer shell solution, 20 wt% PEG with 10 µg/mL BSA-FITC core solution, applied voltage between 12-20 kV and distances between the syringe needle tip and the collector electrode of 12-20 cm. From previous work in our laboratory, outer and inner flow rate combinations of 0.6 ml/hr-0.2ml/hr, and 0.3 ml/hr-0.1ml/hr were selected because they produced good quality fibres with a narrow diameter distribution [101]. It is important to note that the outer to inner solution flow rates (1:3) is consistent with the rates reported in the literature [21, 49]. The initial trials using the faster flow rates (OFR 0.6 ml/hr, INF 0.2 ml/hr) tended to yield larger fibres with beading, so all further experiments were completed using the slower flow rates of 0.3 ml/hr and 0.1 ml/hr for the shell and core solutions respectively. Samples prepared using optimized preparation conditions were imaged using LSCM to verify the encapsulation of the fluorescently tagged protein.

Results are shown in Figure 4.1 and Figure 4.2, and the fibres exhibit the expected green fluorescence from encapsulated BSA-FITC protein.

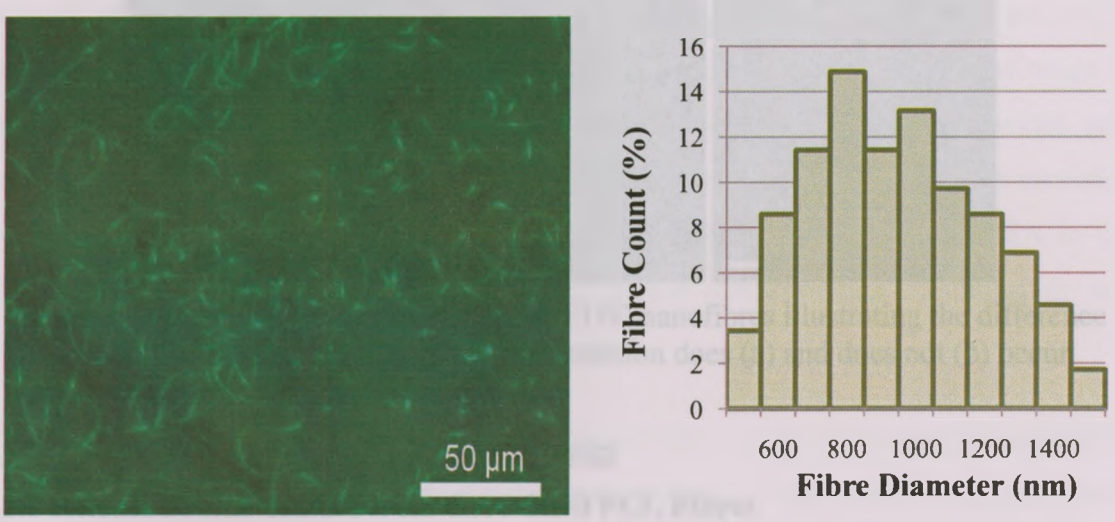

Figure 4.1: Confocal image of PCL/BSA-FITC nanofibres and fibre diameter distribution, with an average fibre diameter was 1069 ± 388 nm (n = 175).

The average fibre diameter of the PCL-BSA core-shell fibres was 1069 ± 388 nm, which is comparable with the 0.8-5.5 µm range of demonstrated in literature [85, 105]. It is important to note that PCL does not fluoresce under confocal microscopy imaging conditions therefore all fluorescence seen is attributed to BSA-FITC [84]. Another important observation is the fluorescence appears in the form of small green beads that are unconnected (Figure 4.2a) indicating that the entire fibre itself is not fluorescing. This suggests that there is no significant mixing between the core and shell solutions in the electrospinning process resulting in a distinct core-shell structure. These results based on PCL-BSA core shell fibres establish the necessary foundation to reach the main goal of this work, which is the localized delivery of bioactive proteins via hollow type I collagen nanofibres.

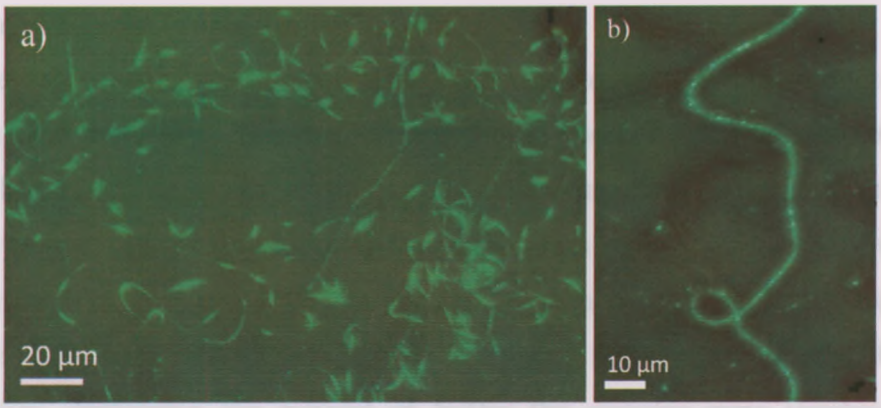

Figure 4.2: Confocal images of PCL/BSA-FITC nanofibres illustrating the difference between fibres when beading of the core solution does (a) and does not (b) occur.

4.2 Protein Release from PCL-BSA Fibres

4.2.1 Release Profile of BSA from Core-Shell PCL Fibres

Based on the results in section 4.1, core-shell fibres consisting of PCL-BSA were prepared in the form of scaffolds. These scaffolds had an average mass of 3.6 ± 0.3 mg and contained an average of 62.7 ± 5.7 µg of BSA. Following the procedure outlined in section 3.4.2, the release profile of BSA was determined (Figure 4.3). Over a period of 10 days samples were able to deliver 22.2 ± 1.4 µg of BSA, which is 35.3 ± 2.2 % of theoretically loaded protein. It was found that protein release from PCL-BSA scaffolds demonstrated a Fickian diffusion based profile, with calculated variables and correlation constants summarized in Table 4.1. Details are discussed below.

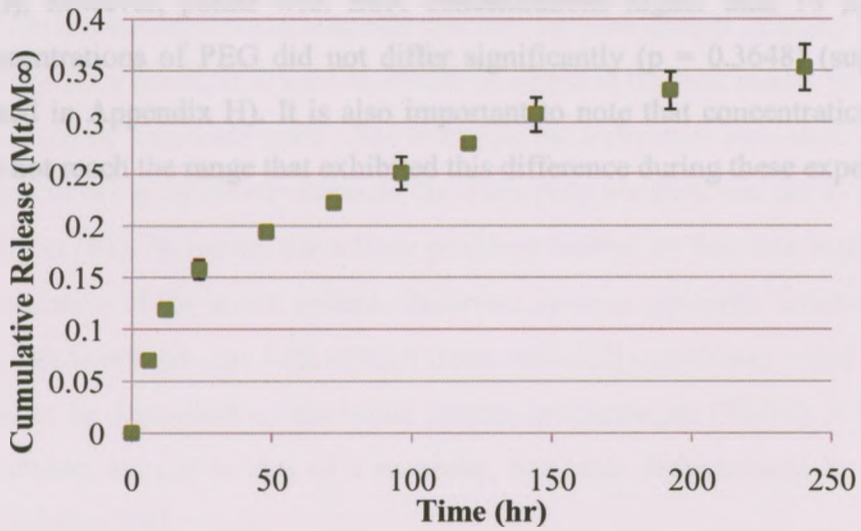

Figure 4.3: Release profile of BSA from PCL core-shell scaffolds. Approximately 35.3 ± 2.2 % of theoretically loaded protein was released at 37 °C over 10 days.

4.2.2 Protein Release Procedure Discussion

For release experiments, the Bradford assay was used to quantify the amount of protein released at each time point. This method was chosen because it is well established in the literature, has a high degree of sensitivity and can be modified to decrease the range of detectable amounts of protein down to the micro gram scale (1-25 μg/mL), which was needed for these experiments [106]. In addition, experimental conditions were modified to increase assay sensitivity. These include increasing the concentration of BSA in the core solution, decreasing the amount of buffer the samples were incubated in and increasing the time between sample collections.

Other assays used for measuring microgram quantities of protein, like the Bicinchoninic Acid (BCA) Microassay and Lowry Assay, have also been widely used in the literature; however, a recent publication indicated that the presence of PEG in the fibres can influence the precision of these assays [84]. In order to assess if PEG influenced the accuracies of the Bradford assay, experiments were carried out using various combinations of PEG and BSA and analyzed. In the end, it did not appear that the concentration of PEG influenced the accuracy of the data over the range of BSA concentrations used in the current set of experiments (Figure 4.4). There was only one concentration of BSA (16 μg/mL) that was significantly different ($p = 0.0158$, using paired t-test for comparing means) from the control (0 μg/mL PEG) and the sample (500 μg/mL PEG); however, points with BSA concentrations higher than 16 μg/mL with varying concentrations of PEG did not differ significantly ($p = 0.3648$) (supplemental data is located in Appendix H). It is also important to note that concentrations of BSA and PEG do not reach the range that exhibited this difference during these experiments.

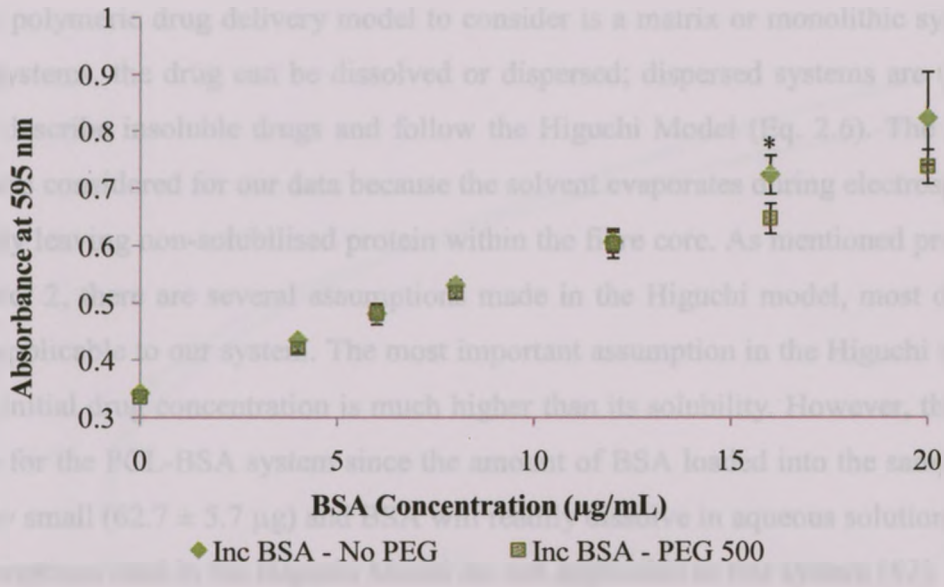

Figure 4.4: The influence of PEG on BSA absorbance was analyzed using Bradford Assay by scanning several samples composed of the same amounts of BSA and varying amounts of PEG. Only one data point showed a significant difference between samples with and without PEG ($p = 0.0158$). Legend: Inc BSA–No PEG = 0-25 µg/mL BSA, 0 µg/mL PEG, Inc BSA-PEG 500 = 0-25 µg/mL BSA, 500 µg/mL PEG.

4.2.3 Protein Release Data Interpretation

Currently in the literature, very few studies have been published which analyze protein release kinetics from electrospun core-shell nanofibres [75, 76, 84]. Controlled release systems of well-defined macroscopic geometries have been thoroughly studied, but translation of that knowledge to nanoscale structures has been limited. This is most likely because, on the macroscopic scale nanocale delivery systems consist of many units of the same geometry. As a result, it is hard to elucidate which is the best model for a delivery system composed of nanoscale units. For example, the individual core-shell fibres have been proposed to act as reservoirs because the outer polymer shell can act as a barrier to control diffusion [84]. However, the release profile exhibited by this data suggests that it is not representative of the entire system. Reservoir systems generally follow zero order kinetics, but this is not the case with release from core-shell nanofibres, which have been demonstrated to be dependent on the initial protein concentration [76-77]. Alternatively, zero order release, similar to that of a reservoir, has been demonstrated from blended electrospun samples [74].

Another polymeric drug delivery model to consider is a matrix or monolithic system. In matrix systems, the drug can be dissolved or dispersed; dispersed systems are typically used to describe insoluble drugs and follow the Higuchi Model (Eq. 2.6). The Higuchi model was considered for our data because the solvent evaporates during electrospinning, ultimately leaving non-solubilised protein within the fibre core. As mentioned previously in Chapter 2, there are several assumptions made in the Higuchi model, most of which are not applicable to our system. The most important assumption in the Higuchi model is that the initial drug concentration is much higher than its solubility. However, this is not the case for the PCL-BSA system since the amount of BSA loaded into the samples was relatively small (62.7 ± 5.7 μg) and BSA will readily dissolve in aqueous solutions. Thus, the assumptions used in the Higuchi Model are not applicable to this system [82].

To model release from electrospun fibres, several studies assumed the system has a cylindrical geometry and release was occurring via diffusion through the fibre wall. This assumption allows the Power Law (Eq. 2.1) to be applied to our data and is shown in Figure 4.5. The treatment of a nanofibrous mesh as the linear summation of all cylinders in the matrix seems to be the most reasonable model for several reasons. The fibrous mesh has an aspect ratio, which is defined as the ratio of the diameter to the length, closer to an infinite cylinder rather than that of a thin slab. If the ideal case is assumed, with an average fibre diameter of 1069 nm and average fibre length of 1 cm (as defined by the scaffold dimensions), then the resulting aspect ratio is very large and, based on the Power Law model, a value of n = 0.45 is expected [80]. When the best fit to the empirical Power Law was determined, the n and k values were found to be 0.39 and 1.83×10^{-3}, respectively, with a correlation coefficient of 0.995. The obtained n value is lower than expected, so to gain a better understanding of the applicability of the Power Law to our nanofibrous system, the data was fit to the cylinder model with n = 0.45 for comparison (Figure 4.5); the resulting k and R^2 values are presented in Table 4.1.

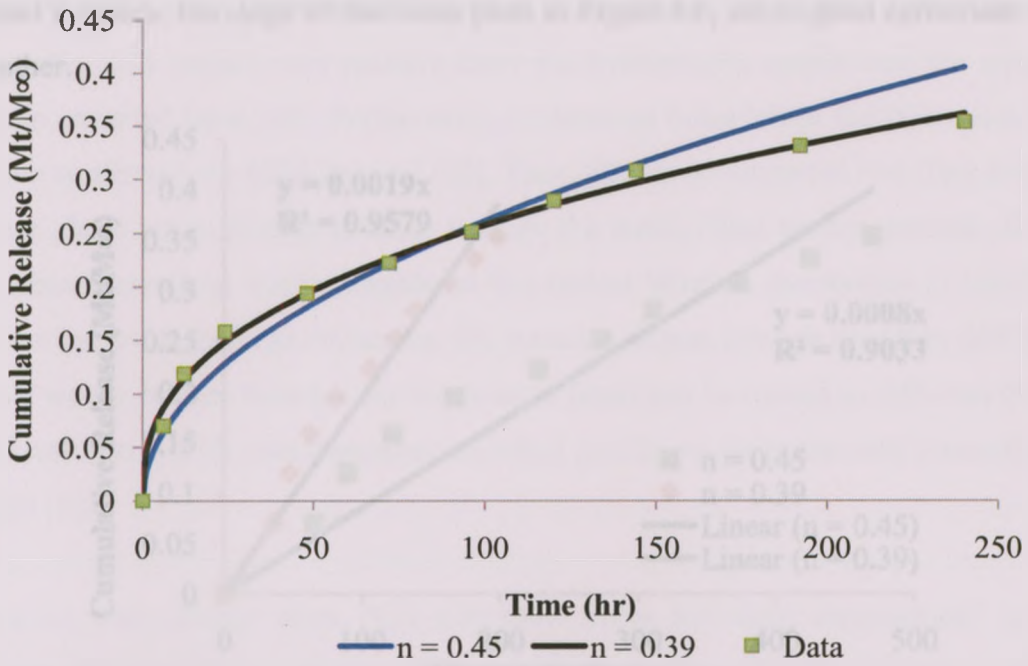

Figure 4.5: Comparison of BSA release from PCL scaffolds (■) to predicted diffusion Power Law model for perfect cylinders, n = 0.45 (–), and best fit model, n = 0.39 (–).

Table 4.1 – Comparison of Power Law Variables n and k Derived from Release Data

	Empirical Diffusion Models	
	Best Fit - Power Law (Eq. 2.1)	*Perfect Cylinder Power Law (Eq. 2.1)*
Equation	$M_t/M_\infty = kt^n$	$M_t/M_\infty = kt^{0.45}$
n	0.39	0.45
k	1.83×10^{-3}	0.80×10^{-3}
D (cm^2s^{-1})	1.88×10^{-15}	0.36×10^{-15}
R^2	0.995	0.983

The curves in Figure 4.5 compare the best fit model (n = 0.39) and the Power Law for cylindrical geometries (n = 0.45). It can be seen that they are very similar demonstrating that the cylindrical model is a plausible and quite reasonable method to describe protein release from our scaffold. Alternatively, the data can be presented linearly where cumulative protein release is plotted as a function of the time to the exponent n. The plotted n values were set at 0.45 for the Power Law for perfect cylinders model and the experimentally derived best fit, which in our case is 0.39. The curve is shown in Figure 4.6. This approach is equivalent to that used to derive the curves in Figure 4.5 and the

obtained k values, the slope of the linear plots in Figure 4.6, are in good agreement with each other.

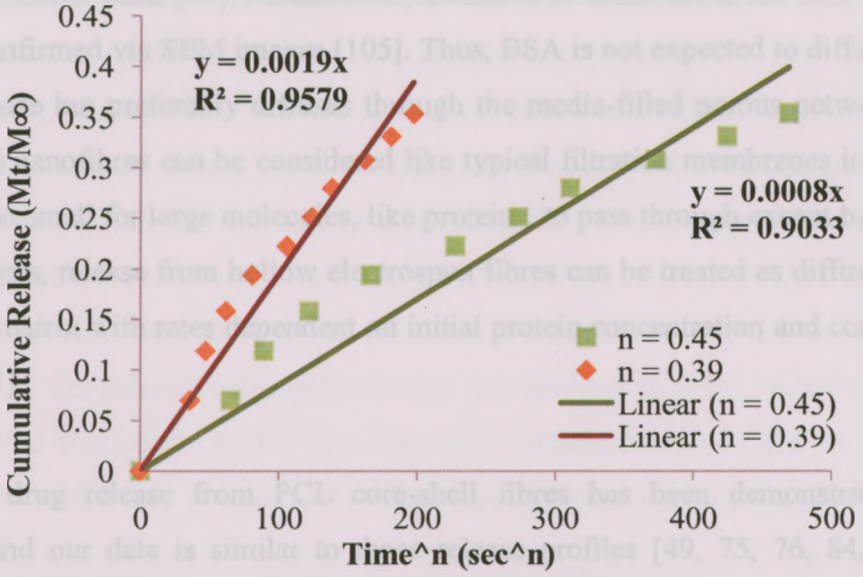

Figure 4.6: Plot of cumulative release of BSA from PCL core-shell scaffolds as a function of time to the exponent n. Samples were plotted with the best fit n = 0.39 (R^2 = 0.958) and the cylindrical Power Law Model n = 0.45 (R^2 = 0.903).

The fitting parameters in the Power Law can be used to estimate a diffusion coefficient, D, for our system using the k value for cylinder geometries shown in Table 2.4. The values for D from the best fit model (n = 0.39) and the cylindrical model (n = 0.45) are summarized in Table 4.1. The diffusion coefficient for both approaches is over a 5-fold range between 0.36-1.88 $x10^{-15}$ cm^2/s. These values compare favourably to a typical diffusion coefficient of ~10^{-15} cm^2/s for proteins [107]. Additionally, Eq. 2.5, diffusion from a cylinder, was considered when selecting models for the protein release data, but the data did not fit. However, this was expected because the model is only accurate for first 20% of release, which is why the Power Law developed by Ritger and Peppas is used because it more accurately describes our set of experimental data [80].

Release of BSA from within PCL fibres represents an interesting release system because water-soluble drugs, like proteins, are not soluble in hydrophobic polymers. Consequently, diffusion of BSA is most likely not occurring through PCL; rather release is anticipated to occur via small pores created by the leaching of PEG, which was

included in the core solution. It has been demonstrated that PEG, which is very hydrophilic, will release very quickly from the hydrophobic matrix into the aqueous media in an initial burst [49]. Furthermore, evidence of holes left in the PCL outer shell has been confirmed via SEM images [105]. Thus, BSA is not expected to diffuse through polymer phase but preferably diffuses through the media-filled porous network. In this sense, these nanofibres can be considered like typical filtration membranes in which the pores are too small for large molecules, like proteins, to pass through except by diffusion. In other words, release from hollow electrospun fibres can be treated as diffusion from a cylindrical matrix with rates dependent on initial protein concentration and concentration gradient [81].

Protein or drug release from PCL core-shell fibres has been demonstrated in the literature, and our data is similar to those release profiles [49, 75, 76, 84, 85, 105]. Previous studies demonstrate approximately 30-40 % release of theoretically loaded protein in 10 days, which corroborates with our data of 35.3 ± 2.2 %. Of the few studies that have applied the Power Law to their data, our experimentally derived n value is in good agreement with the literature (n values of 0.36 - 0.43) [75, 76, 84]. An important distinction between our data and these data is the absence or presence of PEG in the core or shell solutions. As mentioned before, PEG is a porogen and can be used to modulate the release kinetics. For example, studies have shown that the presence of PEG in the polymer shell can increase the release rate compared to samples without PEG [105]. We demonstrate that the presence of PEG in the core solution can also influence the release rate, although not to the same extent as incorporating it into the polymer shell, and this has been corroborated in the literature [84]. Thus, the inclusion of PEG within the core solution during coaxial electrospinning can also be used to modulate the release of proteins from hollow nanofibres. Since the rate of release of each bioactive molecule is specific to its needs during tissue regeneration process, the range of control demonstrated using out approach provides important compliments to methods that have been reported in the literature.

Deviations from the expected n value from the Power Law for cylinders can be attributed to several factors. Polymeric matrix systems have been demonstrated to have some form of burst in the initial stages of release [108]. The main contributors to burst release are process variables, heterogeneity of the matrix and properties of the drug [109]. Imperfections or holes in the fibres are created or redistribution of the drug during solvent evaporation can occur during the electrospinning process [110]. The properties of the drug being released can also influence the release profile. For example, the drugs used in some of the studies were much smaller in size than BSA, which can alter the diffusion kinetics. It has also been shown that BSA has a tendency to redistribute to the shell surface when the solvent evaporates during electrospinning [108]. Another factor to consider is the distribution of the fibre diameters because fibres of different sizes could potentially have different protein and/or PEG loading and consequently, alter the release kinetics.

Controlled delivery of growth factors from TE scaffolds is important because growth factors and their method of delivery play a critical role in the success of tissue regeneration and remodelling. Being able to understand protein release from nanofibrous scaffolds is significant because it presents a method of controlling the rate of tissue development. For example, PDGF is a chemoattractant, meaning that cells will migrate towards it [95, 99]. By releasing PGDF from within the scaffold into the surrounding media, the concentration gradient will trigger the cells to migrate deep into the scaffold, which is important because it will allow remodelling to occur in three dimensions. Additionally, the generation of new tissues is a lengthy process, and by delivering therapeutic growth factors over an extended period of time, the process can be sustained. When extrapolated over 30 and 60 days, the cumulative release of protein from the PCL-BSA scaffold would reach approximately 60 % and 80 % respectively, as estimated based on a diffusion coefficient of $\sim 10^{-15}$ cm^2/s determined in our experiments. By initially drawing cells deep into the scaffold and then maintaining them in a proliferative and migratory state, growth factor delivering scaffolds present a better TE scaffolding material because the majority of the tissue formed will be developed *in-vitro* and be able

to integrate more easily upon implantation. The kinetic analysis presented would allow for the design of bioactive scaffolds not only for AHV leaflet, but for TE in general.

4.3 Growth Factor Release from PCL-PDGF-BB Fibres

Controlled release of BSA from core-shell PCL nanofibres studied in section 4.2 was used to demonstrate and develop an understanding of protein delivery in fibrous scaffolds. This experiment creates an opportunity to develop a bioactive scaffold for tissue engineering by releasing therapeutic proteins, like growth factors, from hollow nanofibres. One of the growth factor that is essential for TE is PDGF-bb, which has been demonstrated to stimulate cell proliferation and migration against its concentration gradient [95, 99]. It is crucial that a reliable and sensitive process is developed to quantify the amount of growth factor released from the fibres. One such method is an ELISA, which can accurately measure growth factor concentrations from 100-2000 pg/ml.

The first step in the growth factor trials was to develop an ELISA protocol and validate it against the PDGF-bb in the core solution. Preliminary tests showed the concentration of PDGF-bb in the core solution was 40-50% less than expected (all ELISA data can be seen in Appendix I), suggesting an error in the standard or protein loss in the core solution. The standard was re-examined and was found to be accurate, so the PDGF-bb core solution was re-evaluated. After a great deal of troubleshooting, the original growth factor was identified as the source of error, and upon using an alternative resource, the accuracy of the assay improved.

Upon optimization of the ELISA, the fabrication core-shell nanofibres containing PDGF-bb was attempted. However, while preparing control core-shell samples (fibres without PDGF-bb) it became apparent that the humidity was influencing the coaxial electrospinning process. In the time at which these samples were being prepared, the relative humidity of the surrounding environment had increased. Increases in humidity cause problems during coaxial electrospinning because increases in the water content in the air prevented the water in the core solution from evaporating during electrospinning.

Samples prepared during this time were composed of wet, beaded and/or woven fibres. To overcome the effect of humidity, the flow rate of the core solution was decreased from 0.1 ml/hr to 0.05 ml/hr in increments 0.01 ml/hr, but smooth, dry fibres could not be produced. Due to time constraints, these experiments could not be explored further; however, some potential solutions include decreasing the water content of the core solution by adding more PEG, or to creating an enclosed environment where the moisture content can be controlled.

4.4 In-vitro Studies

Cell culture studies need to be performed on potential TE scaffolds because they need to be compatible with cells and capable of sustaining cell growth. In this experiment porcine RACs, which are a combination of myofibroblasts and smooth muscle cells, were used as a cell source for *in-vitro* studies. RACs were chosen because they have been established as a viable surrogate cell source for aortic valve tissue regeneration [102, 104]. Initially, *in-vitro* studies used a Sklar Tru-Punch biopsy punch to create circular scaffolds with a diameter of 0.5 cm from PCL-BSA fibres spun onto tinfoil (Figure 4.7a); however several problems were associated with this type of scaffold support. Mainly, the scaffolds would float around in the media and did not provide proper anchorage for the cells. Additionally, the scaffold would peel off the tinfoil, leading to a further decrease in support and affected the reproducibility of the data.

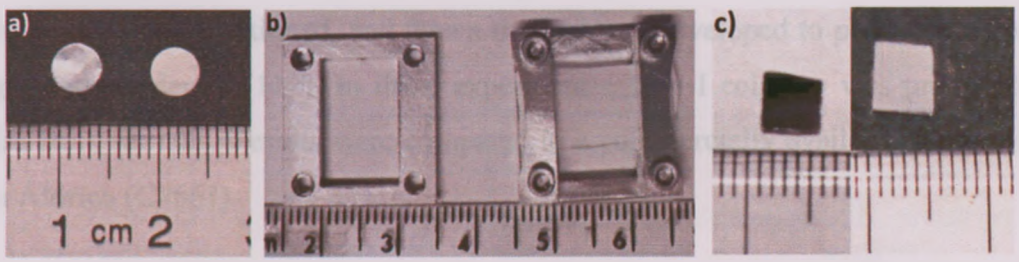

Figure 4.7: Comparison of three types of cell culture supports bare and with fibrous scaffold attached (from left to right): biopsy punch, bioreactor clamps and silicon wafers.

To overcome this, use of bioreactor clamps and silicon wafers were suggested. The square bioreactor clamps create a scaffold area of 1 cm^2 (Figure 4.7b), while the silicon wafers were cut into 0.5 cm^2 squares (Figure 4.7c); both of these offered enough support to prevent the scaffolds from floating freely. The clamps were effective supports, but

there were various associated problems with contamination and microscopy staining. The silicon wafers provided the best support and samples were easily stained. Unfortunately, no PDGF containing scaffolds were able to be produced because of problems associated with the generation of PCL-PDGF scaffolds. The control samples were prepared to develop a standard staining procedure in anticipation for comparison to PDGF-bb containing PCL hollow scaffolds; this data was collected and is presented in Figure 4.8. PCL-BSA scaffolds were able to sustain cell growth over three days, but no definitive conclusions can be drawn from this data due to the lack of a suitable comparison.

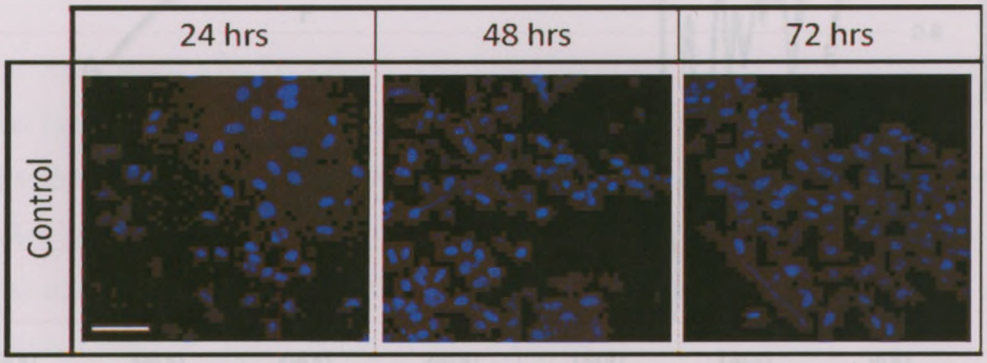

Figure 4.8: Confocal images of control PCL-BSA over 3 days (scale bar = 50 μm).

4.5 Isolation and Purification of Type I Collagen from Rat Tails

Previous work has demonstrated that type I collagen isolated from rat tails is superior to that from calf skin because it creates non-woven fibres with smaller diameters and narrow diameters distributions [111]. Recently, the quality of commercial sources of type I collagen has been questioned, and thus a method was developed to produce and purify collagen independently [112]. In these experiments, type I collagen was produced and purified from rat tails. Results were compared to a commercially available product from Sigma Aldrich (C7661).

Following the procedure outlined in section 3.4.4.2, solid collagen was successfully isolated from rat tails and characterized by FTIR and western blotting. The FTIR spectra of both Sigma and purified collagen samples are in agreement (Figure 4.9) and the prominent peaks present in both samples are summarized in Table 4.2. Notable peaks include the strong amide I and II bands, absorbing around 1650 cm^{-1}, due to the presence of peptide bonds along the polymer backbone and a sharp amide III peak around 1236

cm^{-1} due to the large glycine content (increased CH_2 wagging). All subsequent collagen samples were compared to these spectra as standards to minimize batch to batch variability and can be seen in Appendix J.

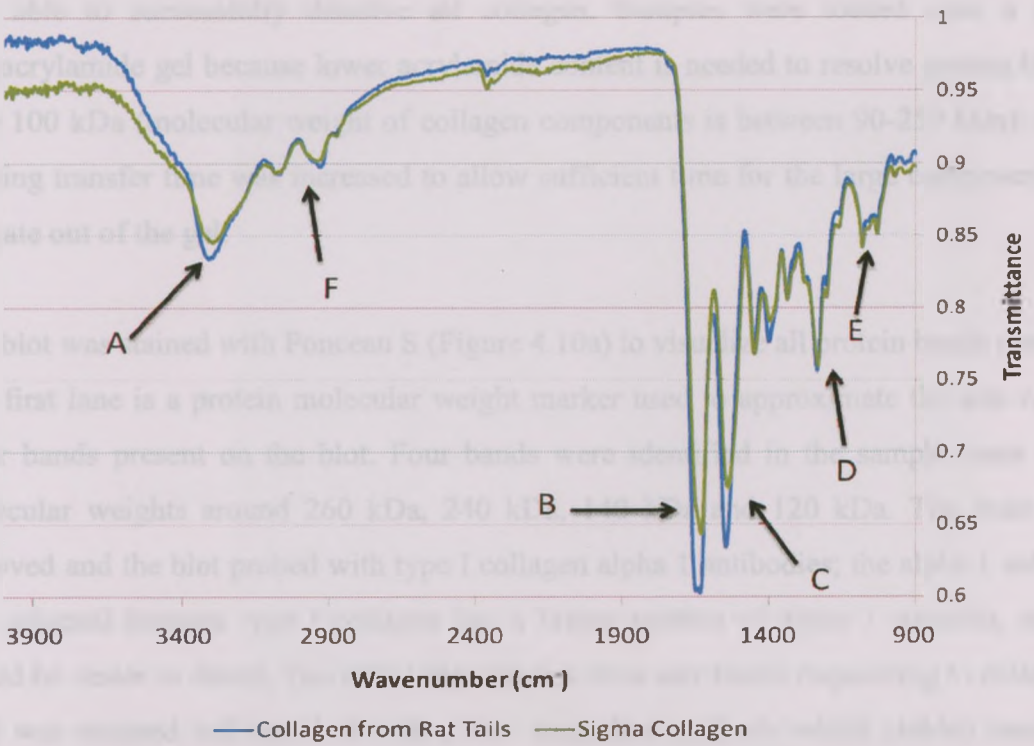

Figure 4.9: FTIR spectra comparing the transmittance of rat tail collagen purchased from Sigma-Aldrich to our purified collagen samples.

Table 4.2 – Summary of FTIR Peaks for Type I Collagen [113-115]

	Expected Value (cm^{-1})	Observed Values* (cm^{-1})	Vibrational Source
A	3300-3330	3307, 3311	N-H Stretching (Amide A)
B	1650-1660	1633, 1650	Amide I, C=O stretching vibrations
C	1530-1560	1540, 1546	Amide II, N-H bending vibrations with C-N Stretching
D	1250-1300 1204-1280	1234, 1236	Amide III, C-CH_2 stretch or CH_2 wagging
E	1031, 1061, 1082	1031, 1081	C-O stretching
F	3067-3077	3077	Amide B (Amide II over tone)

*Observed values are for Sigma and purified samples respectively

Although the FTIR data was in good agreement with the literature, the purity needed to be examined more closely therefore a western blot was performed. A Western blot will be more sensitive because it can detect specific proteins by using antibodies. To perform

the blot, samples must be solubilised and separated by gel electrophoresis. Initial attempts to dissolve collagen in buffer were unsuccessful; however, the use of a tissue homogenizer, which uses mechanical force to break protein into smaller sized fragments, was able to successfully dissolve all collagen. Samples were loaded onto a 6 % polyacrylamide gel because lower acrylamide content is needed to resolve protein bands over 100 kDa (molecular weight of collagen components is between 90-250 kDa); also, blotting transfer time was increased to allow sufficient time for the large components to migrate out of the gel.

The blot was stained with Ponceau S (Figure 4.10a) to visualize all protein bands present. The first lane is a protein molecular weight marker used to approximate the size of the other bands present on the blot. Four bands were identified in the sample lanes with molecular weights around 260 kDa, 240 kDa, 140 kDa and 120 kDa. The stain was removed and the blot probed with type I collagen alpha 1 antibodies; the alpha 1 subunit was selected because type I collagen has a higher portion of alpha 1 subunits, and it would be easier to detect. The initial blot did not show any bands responding to collagen, so it was stripped and reprobed with a new secondary antibody which yielded bands at the 120-140 kDa range (Figure 4.10b).

Type I collagen is composed of three polypeptide chains: two alpha-1 chains and a single alpha-2 chain, both with molecular weights around 70-100 kDa. Also, collagen polypeptide chains have procollagen precursors with higher molecular weights around 150-210 kDa. The stained blot revealed the same banding pattern in the purified and Sigma samples. There were two groups of bands, one set with molecular weights around 240-260 kDa (A) and another around 120-140 kDa (B), and indicated that the purified and Sigma samples contained few containments. When probed with alpha-1 collagen antibodies only the B bands were visualized. This was expected because collagen is composed of several polypeptide chains, so not all bands would correspond to alpha-1 subunits. In addition, the other protein bands could represent other proteins, like the alpha-2 subunits and its procollagen precursor. The B bands located at 120 and 140 kDa correspond to alpha-1 subunits and alpha-1 procollagen respectively. The double banding

pattern occurs because of the presence of the procollagens and has been demonstrated in the literature [116]. The larger A bands are most likely fragments of collagen that did not fully denature and were consequently impeded by the gel.

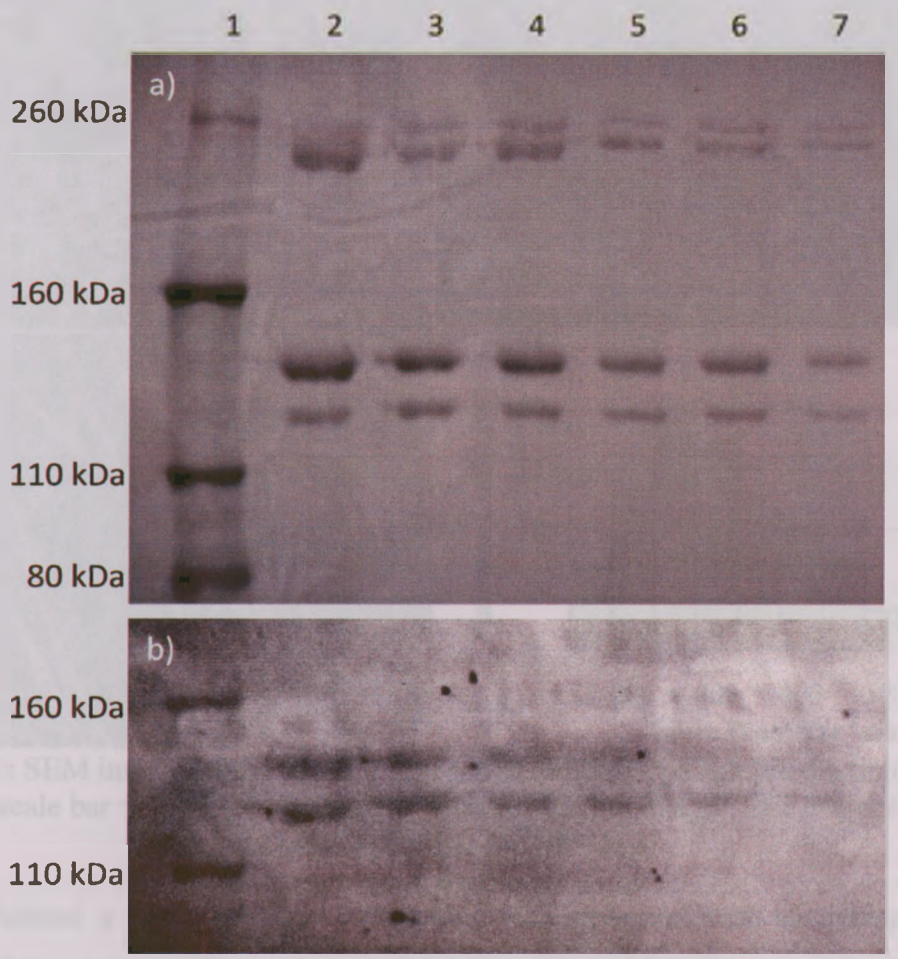

Figure 4.10: Western blot (a) stained with Ponceau S illustrating all protein bands on membrane and (b) probed with rat tail type I collagen alpha-1 antibodies visualizing collagen positive bands. Lane 1 is the pre-stained molecular weight standard. Lanes 2, 4 and 6 contain Sigma-Aldrich as purchased collagen, and lanes 3, 5 and 7 contain purified rat tail collagen in decreasing amounts of 40 µg, 20 µg, and 10 µg, respectively.

4.6 Preparation of Core-shell Type I Collagen Fibres

Following the successful isolation and purification of collagen, the next objective was to create solid and core-shell nanofibres via electrospinning. Unless otherwise stated, our isolated collagen was used to prepare electrospun collagen samples. Stabilized solid collagen nanofibres were prepared using a 5 wt% type I collagen solution, as previously established [111]. Initial attempts to produce solid fibres used a flow rate of 0.15 ml/hr

with a voltage of 24 kV and a distance of 15 cm; the fibres were imaged and are shown in Figure 4.11.

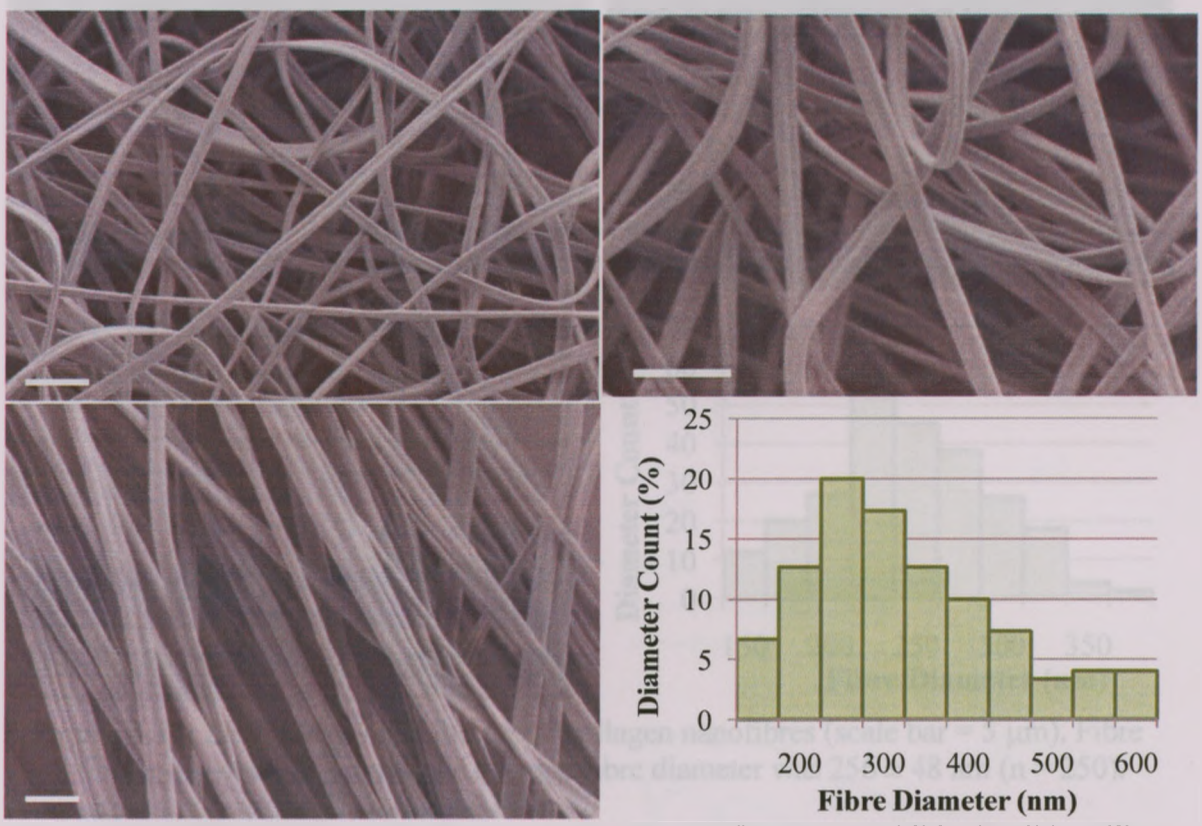

Figure 4.11: SEM images of solid type I collagen nanofibres that exhibited a ribbon like structure (scale bar = 2 μm for top images, 1 μm for bottom image). The average fibre diameter was 349 ± 141 nm (n = 150).

Samples exhibited a flat appearance with ribbon-like structures with an average fibre diameter of 349 ± 141 nm. The presence of flat fibres caused broadening of the diameter distribution. Normally, the solvent evaporates during electrospinning uniformly yielding cylindrical fibres. Ribbons are produced when the solvent evaporates too quickly, causing the surface to harden and the fibre to collapse upon itself [117]. To overcome this, the flow rate was raised to 0.25 ml/hr and the voltage was lowered to 18 kV. This yielded fibres with a more cylindrical appearance, and a smaller average diameter and diameter distribution of 256 ± 48 nm (Figure 4.12).

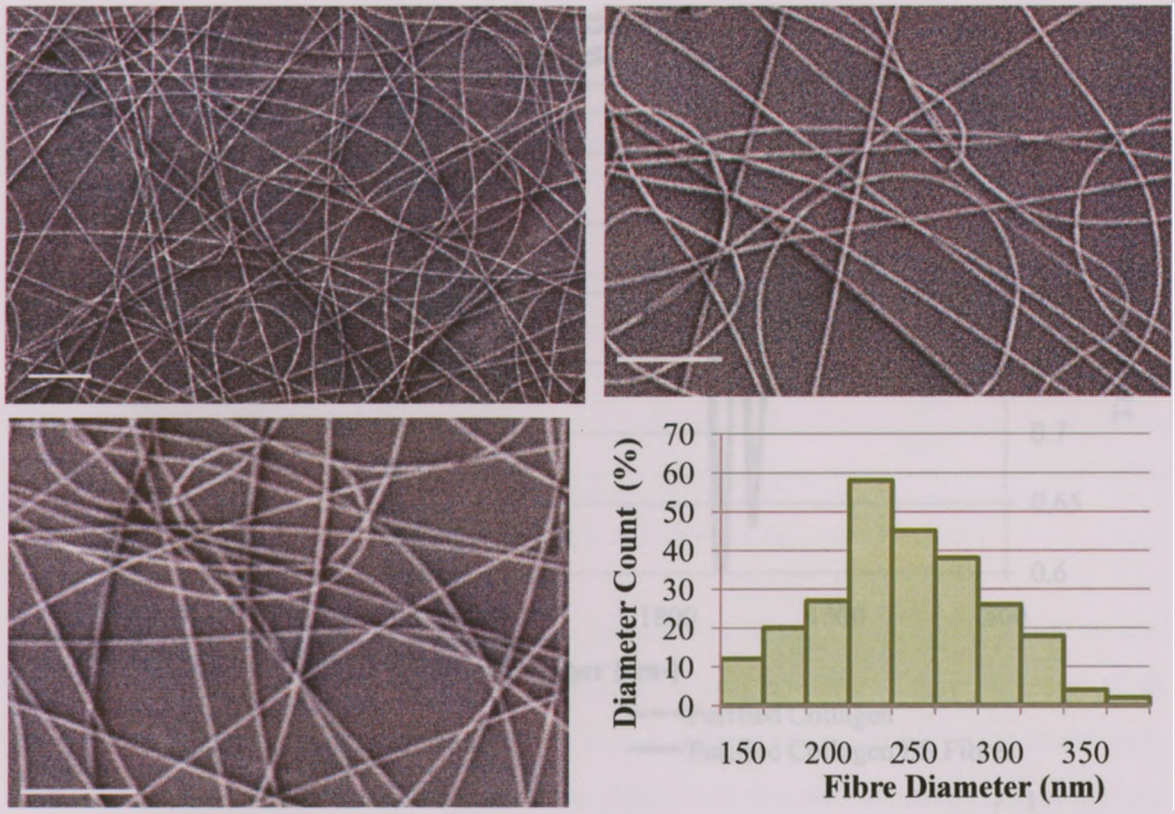

Figure 4.12: SEM images of solid type I collagen nanofibres (scale bar = 5 μm). Fibre diameter distribution determined average fibre diameter was 256 ± 48 nm (n = 250).

Once fibres were successfully produced, the effect of electrospinning on the collagen structure was evaluated using FTIR. Both Sigma and our purified collagen were electrospun and IR spectra of the nanofibrous meshes were obtained; a comparison of electrospun collagen to that of the pre-processed collagen is shown in Figure 4.13. The strong peaks corresponding to the amide groups are still present; however, there are several small peaks present in the electrospun samples in the 1000 - 600cm^{-1} region. These peaks, summarized in Table 4.3, correspond to the solvent HFIP (IR spectra in Appendix K). The HFIP may not have had enough time to fully evaporate because the samples were analyzed very shortly after spinning. Given the volatility of HFIP (boiling point of 58.2°C) it is reasonable to expect that it will evaporate over time. Furthermore, samples of electrospun collagen from previous group members that had given enough time between sample preparation and FTIR reading did not show these peaks [118].

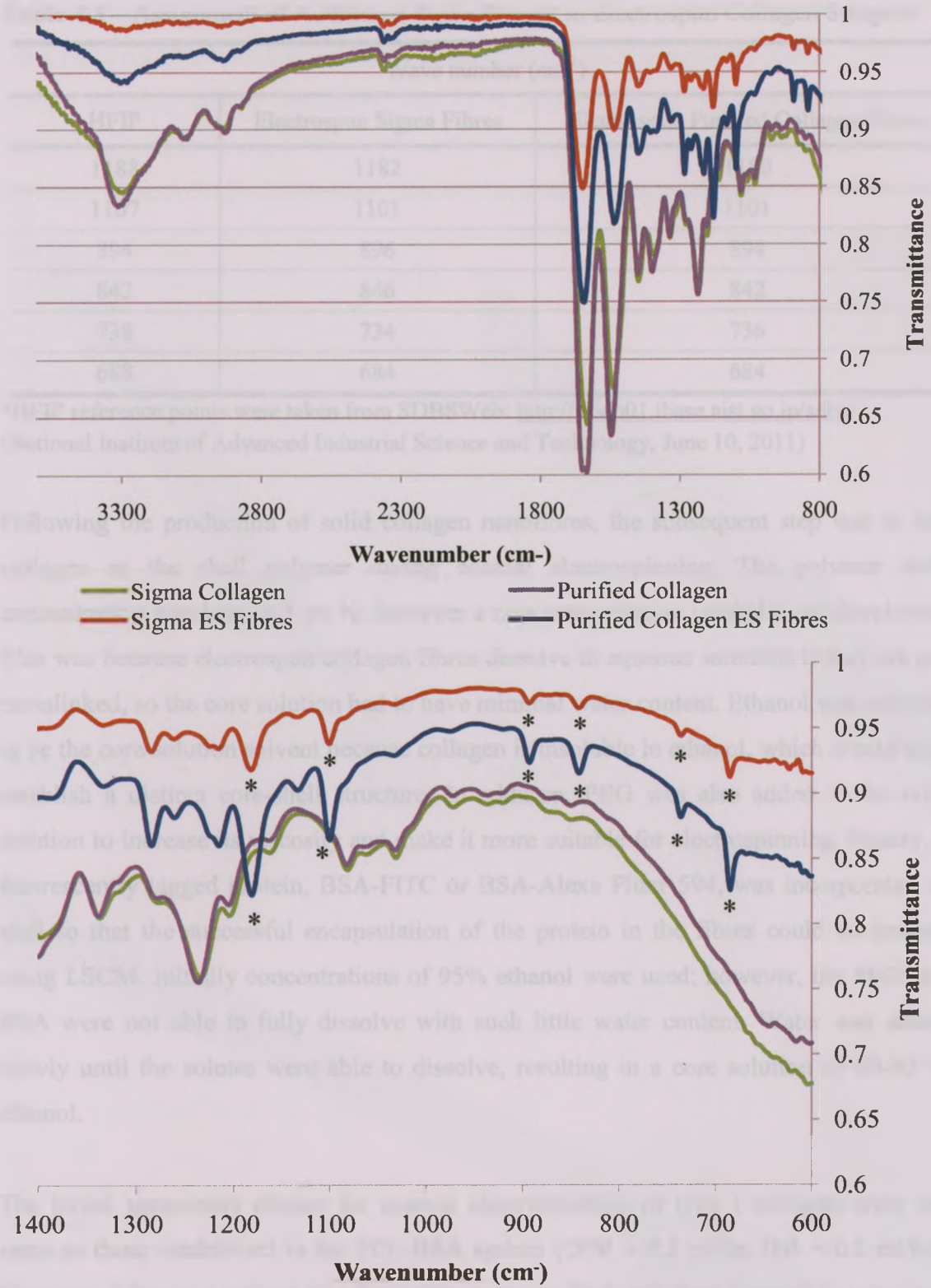

Figure 4.13: FTIR spectra comparing rat tail collagen samples (Sigma-Aldrich and purified samples) before electrospinning and as electrospun fibrous mats. * Peaks are attributed to HFIP.

Table 4.3 – Assignment of Additional Peaks Present in Electrospun Collagen Samples

Wave number (cm^{-1})		
HFIP	Electrospun Sigma Fibres	Electrospun Purified Collagen Fibres
1188	1182	1180
1107	1101	1101
894	896	894
842	846	842
738	734	736
688	684	684

*HFIP reference points were taken from SDBSWeb: http://riodb01.ibase.aist.go.jp/sdbs/ (National Institute of Advanced Industrial Science and Technology, June 10, 2011)

Following the production of solid collagen nanofibres, the subsequent step was to use collagen as the shell polymer during coaxial electrospinning. The polymer shell concentration was kept at 5 wt %; however a new core solution needed to be developed. This was because electrospun collagen fibres dissolve in aqueous solutions if they are not crosslinked, so the core solution had to have minimal water content. Ethanol was selected to be the core solution solvent because collagen is insoluble in ethanol, which would help establish a distinct core-shell structure. In addition, PEG was also added to the core solution to increase its viscosity and make it more suitable for electrospinning. Finally, a fluorescently tagged protein, BSA-FITC or BSA-Alexa Fluor 594, was incorporated as well so that the successful encapsulation of the protein in the fibres could be imaged using LSCM. Initially concentrations of 95% ethanol were used; however, the PEG and BSA were not able to fully dissolve with such little water content. Water was added slowly until the solutes were able to dissolve, resulting in a core solution of 80-90 % ethanol.

The initial parameters chosen for coaxial electrospinning of type I collagen were the same as those established in the PCL-BSA system (OFR = 0.3 ml/hr, IFR = 0.1 ml/hr). However, it became evident that these rates were too high and were lowered to outer and inner rates of 0.24 ml/hr and 0.08 ml/hr. It is important to note that the ratio of the flow rates was always kept constant at 3:1. This produced fibres that appeared wet with lots of

beads, so the flow rates were lowered to 0.18 ml/hr (outer) and 0.06 ml/hr (inner). These rates yielded fibres with a smoother appearance and were subsequently sent for TEM and LSCM imaging (Sigma collagen). The TEM images (Figure 4.14) revealed a well-defined core-shell structure where the solid portion of the fibres only contained type I collagen. Fibres of this composition have not been reported in literature.

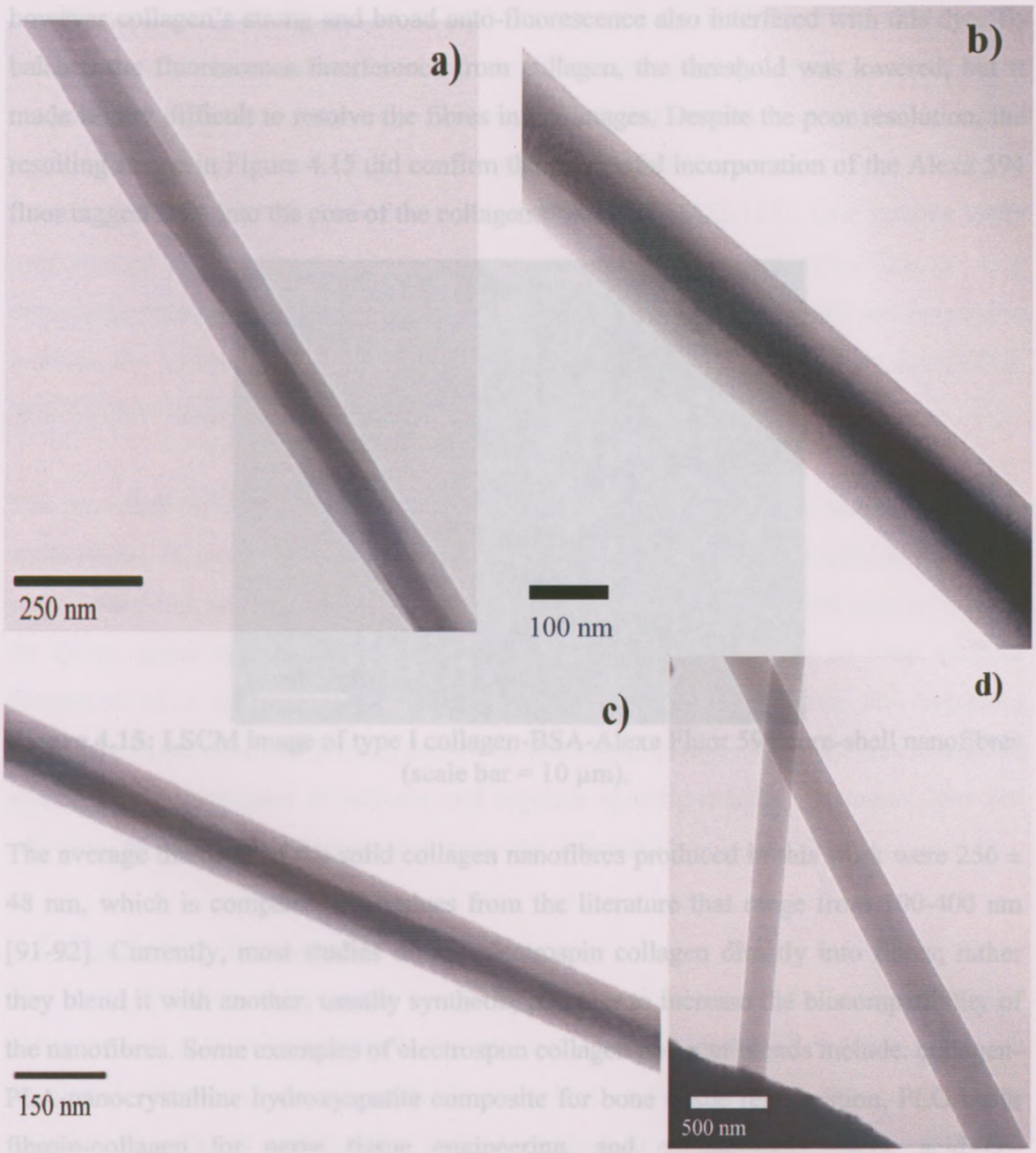

Figure 4.14: TEM images of type I collagen-BSA-FITC core-shell nanofibres (a-c) and solid collagen fibres (d). The average outer and inner fibre diameters are 204 ± 73 nm and 87 ± 33 nm respectively (n = 25).

Collagen is unique in that it is naturally fluorescent, and unfortunately its fluorescence overlaps that of the FITC dye used in these trials, thus no confocal images could be obtained using the BSA-FITC containing fibres. Another fluorescent dye conjugated to BSA used in these experiments was the Alexa 594 Fluor, which emits at a higher wavelength in the red (620 nm). Confocal images were obtained, located in Figure 4.15, however collagen's strong and broad auto-fluorescence also interfered with this dye. To balance the fluorescence interference from collagen, the threshold was lowered, but it made it very difficult to resolve the fibres in the images. Despite the poor resolution, the resulting image in Figure 4.15 did confirm the successful incorporation of the Alexa 594 fluor tagged BSA into the core of the collagen fibres.

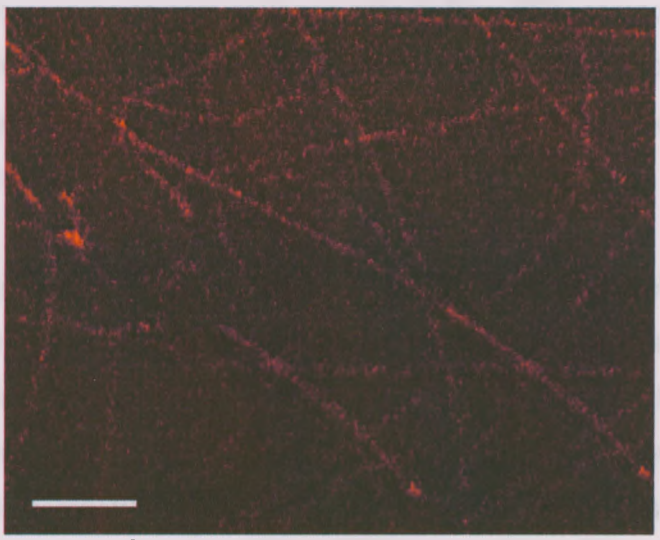

Figure 4.15: LSCM image of type I collagen-BSA-Alexa Fluor 594 core-shell nanofibres (scale bar = 10 μm).

The average diameter of the solid collagen nanofibres produced in this work were 256 ± 48 nm, which is comparable to values from the literature that range from 100-400 nm [91-92]. Currently, most studies do not electrospin collagen directly into fibres; rather they blend it with another, usually synthetic, polymer to increase the biocompatibility of the nanofibres. Some examples of electrospun collagen polymer blends include: collagen-PLA-nanocrystalline hydroxyapatite composite for bone tissue regeneration, PLGA-silk fibroin-collagen for nerve tissue engineering, and collagen-poly(l-lactic acid)-co-poly(caprolactone) for stem cell differentiation [119-121]. Although this approach

generates stable collagen containing fibres, scaffolds from these fibres would not have the same properties as those derived from collagen alone.

Core-shell nanofibres composed of type I collagen shell have not been demonstrated in the literature. The average outer and inner fibre diameters of the hollow type I collagen nanofibres were 204 ± 73 nm and 87 ± 33 nm respectively. There have been few studies published that have used collagen for coaxial electrospinning; however, all of those studies have a synthetic polymer as the core. Essentially, coaxial electrospinning is used as a method of depositing collagen on the surface of synthetic polymeric nanofibres, and examples include thermoplastic polyurethanes and PCL [122-123]. One notable study used coaxial electrospinning to coat collagen onto hollow PCL composite fibres creating nanofibres with three distinct components [110]. Although this approach can be used to increase the biocompatibility of synthetic scaffolds, controlled release from these fibres would not be applicable.

The core-shell collagen nanofibres demonstrated in this work are novel and have multiple applications in the biomedical field. The fibres can be made into scaffolds for tissue engineering and, since they are hollow, they can be used as a controlled delivery device for drugs, genes and proteins. This material lays the foundation for an ideal scaffold composed of a biocompatible, bioactive material. By encapsulating and releasing signalling molecules, like growth factors or cytokines, from inside the fibres a scaffold system can be designed to activate and regulate specific cellular responses, like cell adhesion, proliferation, migration and stem cell differentiation.

4.7 Concluding Remarks

The main objective of this work was to create core-shell nanofibres composed type I collagen and encapsulated growth factors; unfortunately these fibres have yet to be developed. However, several methods have been established that are necessary to complete in order to achieve this goal. A method for isolating and purifying type I collagen from rat tails has been validated and solid nanofibres composed of our purified collagen have been prepared. Core-shell nanofibres composed of either PCL or type I

collagen as the shell and encapsulated model protein BSA have been developed. Furthermore, controlled release from PCL-BSA scaffolds has been demonstrated and a thorough understanding of protein release from PCL core-shell fibres has been established. Following this work, encapsulation and release of PDGF-bb from PCL can be examined using the ELISA protocol developed in this work. Concurrently, *in-vitro* studies comparing the performance of PCL-PDGF scaffolds to PCL-BSA scaffold can be evaluated using the culturing and staining protocols developed here. Next, this system would be adjusted such that encapsulation and release of BSA and PDGF-bb from type I collagen could be examined and in-vitro studies performed.

Chapter 5: Conclusions and Future Work

5.1 Conclusions

Protein encapsulation within core-shell nanofibres was successfully demonstrated. Fibres composed of PCL and encapsulated BSA or BSA-FITC were electrospun and had an average diameter of 1069 ± 388 nm. Scaffolds composed of PCL-BSA, with an average weight of 3.6 ± 0.3 mg, containing an average of 62.7 ± 5.7 μg of BSA were able to deliver approximately 22.2 ± 1.4 μg of BSA, or 35.3 ± 2.2 % of the theoretical loaded protein over 10 days at 37 °C. It was found that protein release from PCL-BSA scaffolds demonstrated Fickian diffusion profiles based on a cylindrical geometry. Additionally, the inclusion of PEG within the core solution during coaxial electrospinning has been demonstrated as a viable method for controlling protein release kinetics from hollow nanofibres. Finally, these scaffolds were tested *in-vitro* and were able to maintain cell adhesion and proliferation over three days.

A method for isolating and purifying type I collagen from rat tails has been developed. The purity and quality of the isolated collagen is comparable to currently available commercial products. This was validated via infrared spectroscopy and western blotting, which generated data equivalent to that in the literature. In turn, the isolated collagen samples were used to prepare solid collagen fibres with an average diameter of 256 ± 48 nm. The FTIR spectra of the electrospun fibres were found to have maintained the same peaks after electrospinning compared to the isolated pre-spun collagen.

Finally, and most significantly, core-shell nanofibres composed of type I collagen and BSA encapsulated have been prepared. These fibres had an average fibre inner and outer diameter of 87 ± 33 nm and 204 ± 73 nm respectively, as determined from TEM images. These fibres are an ideal substrate for TE because they would be biocompatible, biodegradable and capable of localized protein delivery.

5.2 Future Work

This study has demonstrated that controlled release from a tissue engineered scaffold is capable. The next step from this work is to elucidate and analyze the release of PDGF-bb from PCL core-shell fibres using the previously developed ELISA protocol. Next, other growth factors, such as transforming growth factor beta or basic fibroblast growth factor, can be encapsulated in a PCL shell. The release kinetics can be analyzed and their performance *in-vitro* evaluated. Furthermore, scaffolds can be made with random and aligned nanofibre patterns to better mimic the native leaflet layers the ventricularis and fibrosa respectively.

The next stage would be to make these bioactive scaffolds more biocompatible by using native valve ECM components, like type I collagen and hyaluronic acid, as the polymer shell. As demonstrated in this work, core-shell type I collagen fibres can be created; however, because collagen is soluble in media, the fibres need to be crosslinked to increase their stability. Crosslinking will have to be experimentally investigated to determine optimal degree of crosslinks needed to maintain stability but not crosslink the proteins in the core. Once a reliable crosslinking protocol has been established, controlled release from the scaffold can be evaluated. It is hypothesized that scaffolds with higher degree of crosslinking will have slower release rates. Thus, scaffolds with varying degrees of crosslinking will need to be compared to determine if and how much influence crosslinking has on the release rate. Determining how crosslinking effects release rate can be beneficial for these studies because the release kinetics can be optimized to mimic that of natural tissue regeneration.

Finally, the core-shell collagen scaffolds would be evaluated *in-vitro*. They will be assessed in terms of cell proliferation and migration through a variety of cell viability assays. Additionally, cell phenotype and gene expression can be monitored using real time polymerase chain reaction (RT-PCR). It is anticipated that the bioactive collagen-growth factor scaffold will allow cells to penetrate and grow deep within the fibrous scaffold, and ultimately lead to an improved aortic heart valve replacement.

Chapter 6: References

1. Schoen, F. J., & Levy, R. J. (1999). Tissue heart valves: Current challenges and future research perspectives. *Journal of Biomedical Materials Research, 47*(4), 439-465.
2. Quaglia, F. (2008). Bioinspired tissue engineering: The great promise of protein delivery technologies. *International Journal of Pharmaceutics, 364*(2), 281-297.
3. Ma, P. X. (2008). Biomimetic materials for tissue engineering. *Advanced Drug Delivery Reviews, 60*(2), 184-198.
4. Babensee, J. E., McIntire, L. V., & Mikos, A. G. (2000). Growth factor delivery for tissue engineering. *Pharmaceutical Research, 17*(5), 497-504.
5. Schoen, F. (2008). Evolving concepts of cardiac valve dynamics: The continuum of development, functional structure, pathobiology, and tissue engineering. *Circulation, 118*(18), 1864-80.
6. Hjortnaes, J., Bouten, C. V. C., Van Herwerden, L. A., Gründeman, P. F., & Kluin, J. (2009). Translating autologous heart valve tissue engineering from bench to bed. *Tissue Engineering Part B: Reviews, 15*(3), 307-317.
7. Misfeld, M., & Sievers, H. (2007). Heart valve macro- and microstructure. *Philosophical Transactions of the Royal Society B: Biological Sciences, 362*(1484), 1421-1436.
8. Khan, Z., Boughner, D. R., & Lacefield, J. C. (2008). Anisotropy of high-frequency integrated backscatter from aortic valve cusps. *Ultrasound in Medicine & Biology, 34*(9), 1504-1512.
9. Bonow RO, Carabello B, de Leon AC, Edmunds LH, Fedderly MD, & Freed Md. (1998). Guidelines for the management of patients with valvular heart disease. *Circulation, 98*, 1949-84.
10. Yacoub, M. H., & Cohn, L. H. (2004). Novel approaches to cardiac valve repair. *Circulation, 109*(9), 1064-1072.
11. Stewart, B. Fendley, Siscovick, David, Lind ,Bonnie K., Gardin, Julius M., Gottdiener, John S., Smith, M.,Vivienne E., Kitzman, Dalane W. and Otto, Catherine M. (1997). Clinical factors associated with calcific aortic valve disease. *Journal of the American College of Cardiology, 29*(3), 630-634.

12. Rabkin, E., & Schoen, F. J. (2002). Cardiovascular tissue engineering. *Cardiovascular Pathology: The Official Journal of the Society for Cardiovascular Pathology, 11*(6), 305-317.
13. Butany, J., & Leask, R. (2001). The failure modes of biological prosthetic heart valves. *Journal of Long-Term Effects of Medical Implants, 11*(3-4), 115-135.
14. Zilla, P., Brink, J., Human, P., & Bezuidenhout, D. (2008). Prosthetic heart valves: Catering for the few. *Biomaterials, 29*(4), 385-406.
15. Vesely, I. (2003). The evolution of bioprosthetic heart valve design and its impact on durability. *Cardiovascular Pathology, 12*(5), 277-286.
16. Formhals A. (1934) US Patent No. 1,975,504. Washington D, C: U.S. Patent and Trademark Office.
17. Ashammakhi, N., Ndreu, A., Yang, Y., Ylikauppila, H., & Nikkola, L. (2008). Nanofiber-based scaffolds for tissue engineering. *European Journal of Plastic Surgery,* 1-15. DOI: 10.1007/s00238-008-0217-3.
18. Deitzel, J. M., Kleinmeyer, J., Harris, D., & Beck Tan, N. C. (2001). The effect of processing variables on the morphology of electrospun nanofibers and textiles. *Polymer, 42*(1), 261-272.
19. Hardick, O., Stevens, B., & Bracewell, D. (2011). Nanofibre fabrication in a temperature and humidity controlled environment for improved fibre consistency. *Journal of Materials Science, 46*(11), 3890-3898.
20. Zhang, Y., Lim, C., Ramakrishna, S., & Huang, Z. (2005). Recent development of polymer nanofibers for biomedical and biotechnological applications. *Journal of Materials Science: Materials in Medicine, 16*(10), 933.
21. Chakraborty, S., Liao, I., Adler, A., & Leong, K. W. (2009). Electrohydrodynamics: A facile technique to fabricate drug delivery systems. *Advanced Drug Delivery Reviews, 61*(12), 1043-1054.
22. Kenawy, E., Abdel-Hay, F. I., El-Newehy, M. H., & Wnek, G. E. (2009). Processing of polymer nanofibers through electrospinning as drug delivery systems. *Materials Chemistry and Physics, 113*(1), 296-302.

23. Li, W., Laurencin, C. T., Caterson, E. J., Tuan, R. S., & Ko, F. K. (2002). Electrospun nanofibrous structure: A novel scaffold for tissue engineering. *Journal of Biomedical Materials Research, 60*(4), 613-621.
24. Pham, Q. P., Sharma, U., & Mikos, A. G. (2006). Electrospinning of polymeric nanofibers for tissue engineering applications: A review. *Tissue Engineering, 12*(5), 1197-1211.
25. Shin, Y. M., Hohman, M. M., Brenner, M. P., & Rutledge, G. C. (2001). Experimental characterization of electrospinning: The electrically forced jet and instabilities. *Polymer, 42*(25), 09955-09967.
26. Taylor, G. (1969). Electrically driven jets. *Proceedings of the Royal Society of London.A.Mathematical and Physical Sciences, 313*(1515), 453-475.
27. Hohman, M., Shin, M., Rutledge, G., & Brenner, M. (2001). Electrospinning and electrically forced jets. I. stability theory. *Physics of Fluids, 13*(8), 2201-2220.
28. Shin, Y., Hohman, M., Brenner, M., & Rutledge, G. (2001). Electrospinning: A whipping fluid jet generates submicron polymer fibers. *Applied Physics Letters, 78*(8), 1149-1151.
29. Fong, H., Chun, I., & Reneker, D. H. (1999). Beaded nanofibers formed during electrospinning. *Polymer, 40*(16), 4585-4592.
30. Fong, H., & Reneker, D. H. (1999). Elastomeric nanofibers of styrene–butadiene–styrene triblock copolymer. *Journal of Polymer Science Part B: Polymer Physics, 37*(24), 3488-3493.
31. Mit-uppatham, C., Nithitanakul, M., & Supaphol, P. (2004). Ultrafine electrospun polyamide-6 fibers: Effect of solution conditions on morphology and average fiber diameter. *Macromolecular Chemistry and Physics, 205*(17), 2327-2338.
32. Geng, X., Kwon, O., & Jang, J. (2005). Electrospinning of chitosan dissolved in concentrated acetic acid solution. *Biomaterials, 26*(27), 5427-5432.
33. Zong, X., Kim, K., Fang, D., Ran, S., Hsiao, B. S., & Chu, B. (2002). Structure and process relationship of electrospun bioabsorbable nanofiber membranes. *Polymer, 43*(16), 4403-4412.

34. Casper, C. L., Stephens, J. S., Tassi, N. G., Chase, D. B et al. (2004). Controlling surface morphology of electrospun polystyrene fibers: Effect of humidity and molecular weight in the electrospinning process. *Macromolecules, 37*(2), 573-578.
35. Venugopal, J., Low, S., Choon, A. T., & Ramakrishna, S. (2008). Interaction of cells and nanofiber scaffolds in tissue engineering. *Journal of Biomedical Materials Research Part B: Applied Biomaterials, 84B*(1), 34-48.
36. Stevens, M. M., & George, J. H. (2005). Exploring and engineering the cell surface interface. *Science, 310*(5751), 1135-1138.
37. Yan, H., Liu, L., & Zhang, Z. (2009). Alignment of electrospun nanofibers using dielectric materials. *Applied Physics Letters, 95*(14), 143114-143114-3.
38. Schnell, E., Klinkhammer, K., Balzer, S., Brook, G., Klee, D., Dalton, P., et al. (2007). Guidance of glial cell. migration and axonal growth on electrospun nanofibers of poly-epsilon-caprolactone and a collagen/poly-epsilon-caprolactone blend. *Biomaterials, 28*(19), 3012-3025.
39. Lee, C. H., Shin, H. J., Cho, I. H., Kang, Y., Kim, I. A., Park, K., et al. (2005). Nanofiber alignment and direction of mechanical strain affect the ECM production of human ACL fibroblast. *Biomaterials, 26*(11), 1261-1270.
40. Choi, J. S., Lee, S. J., Christ, G. J., Atala, A., & Yoo, J. J. (2008). The influence of electrospun aligned poly(ε-caprolactone)/collagen nanofiber meshes on the formation of self-aligned skeletal muscle myotubes. *Biomaterials, 29*(19), 2899-2906.
41. Huang, Z. M., Zhang, Y. Z., Kotaki, M., & Ramakrishna, S. (2003). A review on polymer nanofibers by electrospinning and their applications in nanocomposites. *Composites Science and Technology, 63*(15), 2223-2253.
42. Pan, H., Li, L., Hu, L., & Cui, X. (2006). Continuous aligned polymer fibers produced by a modified electrospinning method. *Polymer, 47*(14), 4901-4904.
43. Gupta, D., Venugopal, J., Prabhakaran, M. P., Dev, V. R. G., Low, S., Choon, A. T., et al. (2009). Aligned and random nanofibrous substrate for the in vitro culture of schwann cells for neural tissue engineering. *Acta Biomaterialia, 5*(7), 2560-2569.
44. Surrao, D. C., Hayami, J. W., Waldman, S. D., & Amsden, B. G. (2010). Self-crimping, biodegradable, electrospun polymer microfibers. *Biomacromolecules, 11*(12), 3624-3629.

45. McCann, J. T., Li, D., & Xia, Y. (2005). Electrospinning of nanofibers with core-sheath, hollow, or porous structures. *Journal of Materials Chemistry, 15*(7), 735-738.

46. Han, X., Huang, Z., He, C., Liu, L., & Wu, Q. (2008). Coaxial electrospinning of PC(shell)/PU(core) composite nanofibers for textile application. *Polymer Composites, 29*(5), 579.

47. Zhang, H., Zhao, C., Zhao, Y., Tang, G., & Yuan, X. (2010). Electrospinning of ultrafine core/shell fibers for biomedical applications. *SCIENCE CHINA Chemistry, 53*(6), 1246-1254.

48. Loscertales, I. G., Barrero, A., Guerrero, I., Cortijo, R., Marquez, M., & Gañán-Calvo, A. M. (2002). Micro/Nano encapsulation via electrified coaxial liquid jets. *Science, 295*(5560), 1695-1698.

49. Liao, I. C., Chew, S. Y., & Leong, K. W. (2006). Aligned core–shell nanofibers delivering bioactive proteins. *Nanomedicine, 1*(4), 465-471.

50. Langer, R., & Vacanti, J. (1993). Tissue engineering. *Science, 260*(5110), 920-926.

51. Mendelson, K., & Schoen, F. J. (2006). Heart valve tissue engineering: Concepts, approaches, progress, and challenges. *Annals of Biomedical Engineering, 34*(12), 1799-1819.

52. Wang, X., Wenk, E., Zhang, X., Meinel, L., Vunjak-Novakovic, G., & Kaplan, D. L. (2009). Growth factor gradients via microsphere delivery in biopolymer scaffolds for osteochondral tissue engineering. *Journal of Controlled Release, 134*(2), 81-90.

53. Place, E. S., Evans, N. D., & Stevens, M. M. (2009). Complexity in biomaterials for tissue engineering. *Nature Materials, 8*, 457-470.

54. Place, E., George, J., Williams, C., & Stevens, M. (2009). Synthetic polymer scaffolds for tissue engineering. *Chemical Society Reviews, 38*(4), 1139-1151.

55. Hoerstrup, S., Sodian, R., Daebritz, S., Wang, J., Bacha, E. A., Martin, D. P., et al. (2000). Functional living trileaflet heart valves grown in vitro. *Circulation, 102*(suppl 3), III-44-III-49.

56. Breuer, C. K., Shinoka, T., Tanel, R. E., Zund, G., Mooney, D. J., Ma, P. X., et al. (1996). Tissue engineering lamb heart valve leaflets. *Biotechnology and Bioengineering, 50*(5), 562-567.

57. Schmidt, D., Dijkman, P. E., Driessen-Mol, A., Stenger, R., Mariani, C., Puolakka, A., et al. (2010). Minimally-invasive implantation of living tissue engineered heart valves A comprehensive approach from autologous vascular cells to stem cells. *Journal of the American College of Cardiology, 56*(6), 510-520.

58. McKay, W., Peckham, S., & Badura, J. (2007). A comprehensive clinical review of recombinant human bone morphogenetic protein-2 (INFUSE(R) bone graft). *International Orthopaedics, 31*(6), 729-734.

59. Macchiarini, P., Jungebluth, P., Go, T., Asnaghi, M. A., Rees, L. E., Cogan, T. A., et al. (2008). Clinical transplantation of a tissue-engineered airway. *The Lancet, 372*(9655), 2023-2030.

60. Muller-Rath R, Gavénis K, Andereya S., Mumme T., Schmidt-Rohlfing B., & Schneider U. (2007). A novel rat tail collagen type-I gel for the cultivation of human articular chondrocytes in low cell density. *The International Journal of Artificial Organs, 30*(12), 1057-1067.

61. Atala, A., Bauer, S. B., Soker, S., Yoo, J. J., & Retik, A. B. (2006). Tissue-engineered autologous bladders for patients needing cystoplasty. *The Lancet, 367*(9518), 1241-1246.

62. Boyd, M., Flasza, M., Johnson, P. A., Roberts, J. S. C., & Kemp, P. (2007). Integration and persistence of an investigational human living skin equivalent (ICX-SKN) in human surgical wounds. *Regenerative Medicine, 2*(4), 363-370.

63. Causa, F., Netti, P., & Ambrosio, L. (2007). A multi-functional scaffold for tissue regeneration: The need to engineer a tissue analogue. *Biomaterials, 28*(34), 5093-5099.

64. Lutolf, M. P., & Hubbell, J. A. (2005). Synthetic biomaterials as instructive extracellular microenvironments for morphogenesis in tissue engineering. *Nature Biotechnology, 23*(1), 47-55.

65. Martins, A., Araújo, J., Reis, R., & Neves, N. (2007). Electrospun nanostructured scaffolds for tissue engineering applications. *Nanomedicine, 2*(6), 929-942.

66. Nisbet, D. R., Forsythe, J. S., Shen, W., Finkelstein, D. I., & Horne, M. K. (2009). Review paper: A review of the cellular response on electrospun nanofibers for tissue engineering. *Journal of Biomaterials Applications, 24*(1), 7-29.

67. Discher, D. E., Janmey, P., & Wang, Y. (2005). Tissue cells feel and respond to the stiffness of their substrate. *Science, 310*(5751), 1139-1143.

68. Pelham, R. J.,Jr, & Wang, Y. L. (1998). Cell locomotion and focal adhesions are regulated by the mechanical properties of the substrate. *The Biological Bulletin, 194*(3), 348-350.

69. Ramirez, F., & Rifkin, D. B. (2003). Cell signaling events: A view from the matrix. *Matrix Biology, 22*(2), 101-107.

70. Langer, R. (1990). New methods of drug delivery. *Science, 249*(4976), 1527-1533.

71. Kanjickal, D. G., & Lopina, S. T. (2004). Modeling of drug release from polymeric delivery systems: A review. *Critical Reviews in Therapeutic Drug Carrier Systems, 21*(5), 345-386.

72. Allen, T. M., & Cullis, P. R. (2004). Drug delivery systems: Entering the mainstream. *Science, 303*(5665), 1818-1822.

73. Saraf, A., Baggett, L. S., Raphael, R. M., Kasper, F. K., & Mikos, A. G. (2010). Regulated non-viral gene delivery from coaxial electrospun fiber mesh scaffolds. *Journal of Controlled Release, 143*(1), 95-103.

74. Zeng, J., Xu, X., Chen, X., Liang, Q., Bian, X., Yang, L., et al. (2003). Biodegradable electrospun fibers for drug delivery. *Journal of Controlled Release, 92*(3), 227-231.

75. Chew, S. Y., Wen, J., Yim, E. K. F., & Leong, K. W. (2005). Sustained release of proteins from electrospun biodegradable fibers. *Biomacromolecules, 6*(4), 2017-2024.

76. Zamani, M., Morshed, M., Varshosaz, J., & Jannesari, M. (2010). Controlled release of metronidazole benzoate from poly ε-caprolactone electrospun nanofibers for periodontal diseases. *European Journal of Pharmaceutics and Biopharmaceutics, 75*(2), 179-185.

77. Luong-Van, E., Grøndahl, L., Chua, K. N., Leong, K. W., Nurcombe, V., & Cool, S. M. (2006). Controlled release of heparin from poly(ε-caprolactone) electrospun fibers. *Biomaterials, 27*(9), 2042-2050.

78. Sahoo, S., Ang, L. T., Goh, J. C., & Toh, S. (2010). Growth factor delivery through electrospun nanofibers in scaffolds for tissue engineering applications. *Journal of Biomedical Materials Research Part A, 93A*(4), 1539-1550.

79. Katti, D. S., Robinson, K. W., Ko, F. K., & Laurencin, C. T. (2004). Bioresorbable nanofiber-based systems for wound healing and drug delivery: Optimization of fabrication parameters. *Journal of Biomedical Materials Research Part B: Applied Biomaterials, 70B*(2), 286-296.

80. Ritger, P. L., & Peppas, N. A. (1987). A simple equation for description of solute release I. fickian and non-fickian release from non-swellable devices in the form of slabs, spheres, cylinders or discs. *Journal of Controlled Release, 5*(1), 23-36.

81. Saltzman, W. M. (2001). *Drug delivery :Engineering principles for drug delivery.* New York: Oxford University Press.

82. Siepmann, J., & Peppas, N. A. (2001). Modeling of drug release from delivery systems based on hydroxypropyl methylcellulose (HPMC). *Advanced Drug Delivery Reviews, 48*(2-3), 139-157.

83. Albertsson, A., & Varma, I. K. (2003). Recent developments in ring opening polymerization of lactones for biomedical applications. *Biomacromolecules, 4*(6), 1466-1486.

84. Ji, W., Yang, F., van den Beucken, J. J. J. P., Bian, Z., Fan, M., Chen, Z., et al. (2010). Fibrous scaffolds loaded with protein prepared by blend or coaxial electrospinning. *Acta Biomaterialia, 6*(11), 4199-4207.

85. Jiang, H., Hu, Y., Zhao, P., Li, Y., & Zhu, K. (2006). Modulation of protein release from biodegradable core–shell structured fibers prepared by coaxial electrospinning. *Journal of Biomedical Materials Research Part B: Applied Biomaterials, 79B*(1), 50-57.

86. Shoulders, M. D., & Raines, R. T. (2010). Collagen structure and stability. *Annual Review of Biochemistry, 0* doi:10.1146/annurev-biochem-78-042110-200001

87. Myllyharju, J., & Kivirikko, K. I. (2001). Collagens and collagen-related diseases. *Ann Med, 33*(1), 7-21.

88. Buehler, M. J. (2006). Nature designs tough collagen: Explaining the nanostructure of collagen fibrils. *Proceedings of the National Academy of Sciences, 103*(33), 12285-12290.

89. Okuyama, K., Okuyama, K., Arnott, S., Takayanagi, M., & Kakudo, M. (1981). Crystal and molecular structure of a collagen-like polypeptide (pro-pro-gly)10. *Journal of Molecular Biology, 152*(2), 427-443.

90. Matthews, J. A., Wnek, G. E., Simpson, D. G., & Bowlin, G. L. (2002). Electrospinning of collagen nanofibers. *Biomacromolecules, 3*(2), 232-238.

91. Sell, S., McClure, M., Garg, K., Wolfe, P., & Bowlin, G. (2009). Electrospinning of collagen/biopolymers for regenerative medicine and cardiovascular tissue engineering. *Advanced Drug Delivery Reviews, 61*(12), 1007-1019.

92. Yang, L., Fitié, C. F. C., van der Werf, K. O., Bennink, M. L., Dijkstra, P. J., & Feijen, J. (2008). Mechanical properties of single electrospun collagen type I fibers. *Biomaterials, 29*(8), 955-962.

93. Carlisle, C. R., Coulais, C., & Guthold, M. (2010). The mechanical stress–strain properties of single electrospun collagen type I nanofibers. *Acta Biomaterialia, 6*(8), 2997-3003.

94. Narine, K., Wever, O. D., Valckenborgh, D. V., Francois, K., Bracke, M., Desmet, S., et al. (2006). Growth factor modulation of fibroblast proliferation, differentiation, and invasion: Implications for tissue valve engineering. *Tissue Engineering, 12*(10), 2707-

95. Pierce, G., Vande Berg, J., Rudolph, R., Tarpley, J., & Mustoe, T. (1991). Platelet-derived growth factor-BB and transforming growth factor beta 1 selectively modulate glycosaminoglycans, collagen, and myofibroblasts in excisional wounds. *American Journal of Pathology, 138*(3), 629-646.

96. Whitaker, M. J., Quirk, R. A., Howdle, S. M., & Shakesheff, K. M. (2001). Growth factor release from tissue engineering scaffolds. *Journal of Pharmacy and Pharmacology, 53*, 1247.

97. Seppä, H., Grotendorst, G., Seppä, S., Schiffmann, E., & Martin, G. R. (1982). Platelet-derived growth factor in chemotactic for fibroblasts. *The Journal of Cell Biology, 92*(2), 584-588.

98. Hart, C., Forstrom, J., Kelly, J., Seifert, R., Smith, R., Ross, R., et al. (1988). Two classes of PDGF receptor recognize different isoforms of PDGF. *Science, 240*(4858), 1529-1531.

99. Bornfeldt, K. E., Raines, E. W., Graves, L. M., Skinner, M. P., Krebs, E. G., & Ross, R. (1995). Platelet-derived growth factor. distinct signal transduction pathways associated with migration versus proliferation. *Ann N Y Acad Sci, 766*, 416-30.

100. Ross, Russell. (1987). Platelet-derived growth factor. *Annual Review of Medicine, 38*(1), 71-79.

101. Haley, J. (2009). Bioactive scaffolds for tissue engineering. *Master's Thesis* (The University of Western Ontario), London, Ontario, Canada.

102. Johnston, D. E., Boughner, D. R., Cimini, M., & Rogers, K. A. (2006). Radial artery as an autologous cell source for valvular tissue engineering efforts. *Journal of Biomedical Materials Research Part A, 78a*(2), 383-393.

103. Bradford, M. M. (1976). A rapid and sensitive method for the quantitation of microgram quantities of protein utilizing the principle of protein-dye binding. *Analytical Biochemistry, 72*(1-2), 248-254.

104. Appleton, A. J. E., Appleton, C. T., Boughner, D. R., & Rogers, K. A. (2009). Vascular smooth muscle cells as a valvular interstitial cell surrogate in heart valve tissue engineering. *Tissue Engineering Part A, 15*(12), 3889-3897.

105. Jiang, H., Hu, Y., Li, Y., Zhao, P., Zhu, K., & Chen, W. (2005). A facile technique to prepare biodegradable coaxial electrospun nanofibers for controlled release of bioactive agents. *Journal of Controlled Release, 108*(2-3), 237-243.

106. Noble, J. E., & Bailey, M. J. A. (2009). Chapter 8 quantitation of protein. In Richard R. Burgess and Murray P. Deutscher (Ed.), *Methods in enzymology* (pp. 73-95) Academic Press.

107. Ho, W. S. W., & Sirkar, K. K. (1992). *Membrane handbook*. New York, NY: Van Nostrand Reinhold.

108. Szentivanyi, A., Chakradeo, T., Zernetsch, H., & Glasmacher, B. (2011). Electrospun cellular microenvironments: Understanding controlled release and scaffold structure. *Advanced Drug Delivery Reviews, 63*(4-5), 209-220.

109. Huang, X., & Brazel, C. S. (2001). On the importance and mechanisms of burst release in matrix-controlled drug delivery systems. *Journal of Controlled Release, 73*(2-3), 121-136.

110. Zhang, Y. Z., Venugopal, J., Huang, Z. M., Lim, C. T., & Ramakrishna, S. (2005). Characterization of the surface biocompatibility of the electrospun PCL-collagen nanofibers using fibroblasts. *Biomacromolecules, 6*(5), 2583-2589.

111. Mekhail, M., Wong, K. K., Padavan, D. T., Wu, Y., O'Gorman, D. B., & Wan, W. (2011). Genepin-crosslinked electrospun collagen nanofibres. *Journal of Biomaterials Science, Polymer Edition,* (14), 10.1163/092050610X538209.

112. Hsieh, A., Zahir, T., Lapitsky, Y., Amsden, B., Wan, W., & Shoichet, M. S. (2010). Hydrogel/electrospun fiber composites influence neural stem/progenitor cell fate. *Soft Matter, 6*(10), 2227-2237.

113. Miyazawa, T., Shimanouchi, T., & Mizushima, S. (1958). Normal vibrations of N-methylacetamide. *The Journal of Chemical Physics, 29*(3), 611-617.

114. Doyle, B. B., Bendit, E. G., & Blout, E. R. (1975). Infrared spectroscopy of collagen and collagen-like polypeptides. *Biopolymers, 14*(5), 937-957.

115. Jackson, M., Choo, L., Watson, P. H., Halliday, W. C., & Mantsch, H. H. (1995). Beware of connective tissue proteins: Assignment and implications of collagen absorptions in infrared spectra of human tissues. *Biochimica Et Biophysica Acta (BBA) - Molecular Basis of Disease, 1270*(1), 1-6.

116. Zeugolis, D. I., Khew, S. T., Yew, E. S. Y., Ekaputra, A. K., Tong, Y. W., Yung, L. L., et al. (2008). Electro-spinning of pure collagen nano-fibres – just an expensive way to make gelatin? *Biomaterials, 29*(15), 2293-2305.

117. Reneker, D. H., & Yarin, A. L. (2008). Electrospinning jets and polymer nanofibers. *Polymer, 49*(10), 2387-2425.

118. Mekhail, M. (2009). Genepin-crosslinked electrospun collagen nanofibres. *Masters Thesis* (The University of Western Ontario), London, Ontario, Canada.

119. Torres-Giner, S., Gimeno-Alcañiz, J. V., Ocio, M. J., & Lagaron, J. M. (2011). Optimization of electrospun polylactide-based ultrathin fibers for osteoconductive bone scaffolds. *Journal of Applied Polymer Science, 122*(2), 914-925.

120. Wang, G., Hu, X., Lin, W., Dong, C., & Wu, H. (2011). Electrospun PLGA–silk fibroin–collagen nanofibrous scaffolds for nerve tissue engineering.*47*(3), 234-240.

121. Jin, G., Prabhakaran, M. P., & Ramakrishna, S. (2011). Stem cell differentiation to epidermal lineages on electrospun nanofibrous substrates for skin tissue engineering. *Acta Biomaterialia, 7*(8), 3113-3122.

122. Chen, J., & Chang, Y. (2011). Preparation and characterization of composite nanofibers of polycaprolactone and nanohydroxyapatite for osteogenic differentiation of mesenchymal stem cells. *Colloids and Surfaces B: Biointerfaces, 86*(1), 169-175.

123. Haslauer, C. M., Moghe, A. K., Osborne, J. A., Gupta, B. S., & Loboa, E. G. (2011). Collagen-PCL sheath-core bicomponent electrospun scaffolds increase osteogenic differentiation and calcium accretion of human adipose-derived stem cells *Journal of Biomaterials Science, Polymer Edition, 22*(13), 1695-1712.

Appendices

Appendix A – Buffers and ELISA Solutions

1X (100 mM) Phosphate Buffered Saline (PBS)

1) Combine the following in 1 litre of distilled water:
   - 1.150 g Sodium phosphate dibasic heptahydrate (8.1 mM)
   - 8.006 g Sodium Chloride (137 mM)
   - 0.204 g Potassium phosphate monobasic (1.5 mM)
   - 0.201 g Potassium Chloride (2.7 mM)
2) Adjust pH to 7.2-7.4

1.5 M Tris Buffered Saline (TBS)

1) Combine the following in 1 litre of distilled water:
   - 8.80 g Sodium Chloride (137 mM)
   - 3.0 g TRIS (tris (hydroxy methyl) aminomethane) Base (1.5 mM)
   - 0.201 g Potassium Chloride (2.7 mM)
2) Adjust pH to:
   - 7.4-7.6 with concentrated hydrochloric acid (HCl)
   - 8.8 with concentrated sodium hydroxide (NaOH)

1X (100 mM) Tris Buffered Saline with TWEEN (TBS-T)

1) Add 500 µL Tween-20 (0.05%) to 1 litre of TBS.
2) Adjust pH to 7.4-7.6

4X Loading Buffer (Laemmli Buffer)

1) Combine the following:
   - 2.0 ml of 1M Tris-HCl
   - 0.8 g of SDS
   - 4.0 ml of 100% glycerol
   - 0.4 ml of 14.7 M β-mercaptoethanol
   - 8.0 mg bromophenol blue
2) Adjust pH to 6.8
3) Add water to a final volume of 10 mL.

10X Running Buffer

1) Combine the following in 1 litre of distilled water:
   - 30.3 g of Tris base
   - 144.0 g of Glycine
   - 10.0 g of SDS
2) Adjust pH to 8.3

Transfer Buffer

1) Add 200 mL of methanol to 800 mL litre of running buffer

Lysis Buffer

1) Combine the following with a final volume of 10 mL:
   - 300 µl 5M NaCl
   - 50 µl 1M Tris, pH 8.0
   - 1 mL Glycerol
   - 8.45 mL nanopure water
   - 100 µl 10% SDS
   - Protease inhibitor (one pellet)
2) Turn on heat block to 95°C.
3) Put on ice to keep buffer cold.

ELISA Solutions

ELISA Wash Buffer

1) Add 500 µL of Tween® 20 (0.05%) in 1 L of 1X PBS
2) Filter sterilize and adjust pH to 7.2-7.4

PDGF-BB ELISA Reagent Diluent

1) Add 10.0 g of BSA (1.0 %) to 1 L 1X PBS
2) Filter sterilize and adjust pH to 7.2-7.4

Substrate Solution - ELISA Substrate Reagent Pack (DY999)

- 1:1 mixture of Colour Reagent A (H_2O_2) and B (Tetramethylbenzidine)

ELISA Stop Solution (2 N H_2SO_4)

- Dilute 5.55 mL of 18 N H_2SO_4 with distilled water to a final volume of 50 mL

Appendix B – Isolation of Type I Collagen from Rat Tails

1) Thaw frozen rats tails in 70% ethanol for 1 hour
2) Use scalpel to cut off tip of tail and expose white collagen fibres. Using forceps pull out collagen fibres from tail and place in separate sterile dish.
3) Continue cutting rat tail in segments, exposing and pulling out fibres, ensuring to clean fibres of contaminating tissue.
4) At this point, fibres can be stored at -20 °C or proceed to collagen solution.
5) Weigh out 4 g/L of fibres (approximately 5 tails) and soak in 200 mL of 70% ethanol for 30 minutes with forceps.
6) Place fibres in sterile Petri dish and leave overnight in a tissue culture hood with UV light on to sterilize fibres.
7) Prepare acetic acid solution (1 mL of concentrated acetic acid in 1 L of distilled water) and filter sterilize.
8) Add 900 mL of acetic acid solution to collagen fibres in an autoclaved 1 litre flask with sterile stir bar. Place on stirrer in cold room (at 4 °C) for 4-7 days to dissolve collagen.
9) Centrifuge the solution at 11, 000 rpm (10, 000 g) for 2 hours at 4 °C with brakes on.
10) Collect supernatant in a sterile bottle and measure protein concentration using Sircol Collagen Assay (should be 1-3 mg/mL)
11) Collagen solution can be stored at this point at 4 °C.
12) To obtain collagen protein powder, freeze small samples (~10-15 ml) overnight in a -20 °C freezer and lyophilize for 1-2 days.

Appendix C – Cell Culture Protocols

PROTOCOL: Isolation of Porcine Radial Artery Cells

Reagents:

- Medium M199 (Sigma Aldrich, cat # M4530)
- M199 (500 mL) + 10% Fetal Bovine Serum (FBS) (50 mL) + 1% Penicillin/Streptomycin (P/S) (5 mL)
- M199 (120 mL) + 0.08% Collagenase (0.0010 ± 0.0001 g) + 1% P/S (1.2 mL = 2 x 600 µL) + 0.25µg/mL Amphotericin B (120 µL = 2 x 60 µ) – solution must be sterile (filter)

Equipment:

- Biohazard Bags
- Dissection tray
- Instruments for dissecting
- Scalpel handles and several #20 blades
- 50 mL Culture tubes
- Sterile Forceps
- Sterile petri dish

How to get pig forelimbs:

1) Contact Sheri Van Lingen at CSTAR (x32358) Sheri.VanLingen@lhsc.on.ca and ask her if/when they will be sacrificing some pigs. Tell her you are interested in taking the forelimbs of those pigs (from the elbow down).
2) Leave a labeled cooler filled with ice in the dead animals room in Animal Care on the day of the pig surgery. Retrieve the following day and use tissues.
3) Make sure you have prepared enough of your solutions before picking up the forelimbs.
4) Make sure limbs remain on ice until you are ready to dissect out the radial arteries.

Protocol:

To be performed outside the tissue culture hood

1) Dissect out radial arteries and place each into a tube containing approx 40 mls of M199.
2) Remove arteries from the tube and place in a petri dish. Ensure extra fat tissues are removed before transferring dish into the tissue culture hood.

To be performed inside the tissue culture hood.

1) Mince arteries into $1mm^3$ pieces with a pair of forceps and a #20 scalpel blade.
2) Place pieces in a new tube containing 40mls of M199 + 0.08% Collagenase + 1% P/S + 0.25µg/mL Amphotericin B solution.
3) Incubate at 37°C for 24 hours, inverting several times throughout the 24 hours.
4) Centrifuge culture tubes for 5 minutes at 1250 RPM.
5) Remove supernatant leaving arteries pieces at the bottom.
6) Plate individual tissue pieces on 3-$100mm^2$ dishes with 10mls of M199 + FBS + P/S.
7) Monitor for cellular outgrowth and remove tissue pieces once sufficient outgrowth has occurred (Approx. 7 days)

PROTOCOL: Thawing Porcine Radial Artery Cells

1) Warm media (DMEM + 10% FBS + 1% P/S) in water bath (35°C, temperature is critical), sterilize using 70% ethanol and place in tissue culture hood
2) Remove frozen cryotube from -80°C freezer
3) Warm cryotube in water bath (35°C, temperature is critical) until mostly thawed (some ice crystals should be visible)
4) Wipe down cryotube with 70% ethanol before placing in tissue culture hood
5) Use the large (blue) micropipette to transfer the contents of the cryotube (1mL) into a 15mL Falcon tube
6) Quickly add approximately 9 mL of media to tube
7) Centrifuge tube for 5 min. at 1250 RPM
8) Remove tube and use glass pipette to suction out as much of the supernatant as possible, leaving the entire pellet (cells) at the bottom
9) Add 9 mL of media to the tube
10) Resuspend the pellet my continuously pipetting and dispensing the media.
    Be careful not to spill the media while doing this as the tube cannot accommodate all of the liquid and the volume displaced by the pipette.
11) Transfer all of the contents from the tube into three $100mm^2$ dishes (3 mL/dish)
12) Add 7 mL of media to each dish and incubate at 37°C, 5% CO_2

PROTOCOL: Counting Cells Using a Hemocytometer

1) Clean hemocytometer and cover slip using a kim wipe and 70% ethanol
2) Use pipette to extract 20 µL of cells in solution (after re-suspending them post-centrifugation)
3) Insert 20 µL into well next to coverslip (direct towards centre of plate)
4) Count areas 1 – 4 (Include cells on top and right-hand border of each area)

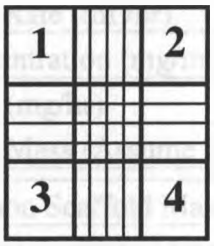

To calculate the number of cells/well:

Average cell = $\frac{(\text{\# cells in areas 1-4}) \times 10^4}{4}$

Volume/well = $\frac{\text{Number of cells/well}}{\text{Average \# cells}}$

PROTOCOL: Fixing and Staining of Radial Artery Cells on Scaffolds

1) Remove media from wells and wash with PBS.
2) Fix using a 10% Formalin solution (3.7% formaldehyde in PBS) for 10 minutes. Wash with PBS and repeat two more times.
3) Prepare mounting media with 500 µL of Vectashield and 500 µL of Hoechst 33342. Vortex to ensure proper mixing.
4) Using sterile forceps gently remove scaffolds from holder and place onto sterile microscope slide.
5) Add ~100 µL of mounting media onto scaffold and top with sterile cover slip.
6) Allow to settle for 10 minutes then image. Can be stored at 4 °C and imaged later.

Appendix D – Theoretical Protein Loading Calculations

These are sample calculations using a 12 wt% PCL in TFE solution for the shell, and 10 mg/mL BSA with 20 wt% PEG in PBS for the core. Assumptions made in calculations are: spinning time is constant for both inner and outer pumps and the mass ratio is constant throughout scaffold.

		PCL	PEG	BSA
Flow Rate (mL/hr)		0.3	0.1	0.1
Concentration (mg/mL)		120	200	10
Mass (mg/hr)		36	20	1
Total Mass (Assume 1 hr)		57		
Fraction Scaffold Mass		0.6316	0.3509	0.0175
Percent Scaffold Mass (%)		63.16	35.09	1.75
Example: Scaffold mass = 5 mg				
	Mass (mg)	3.158	1.754	0.0877
	Mass (ng)	3158	1754	87.7

Appendix E – Bradford Assay and Standard

The Bradford assay is protocol used to determine the amount of protein in sample using its absorbance, and is calculated according to Beer's law, $A = \varepsilon lc$, where l is the path length (1 cm), ε is the molar extinction constant and c is the concentration (μg/mL). This experimental setup is for a 96-well plate with a final volume of 200 μL.

1) Prepare BSA protein standards according to the following chart:

[BSA] (μg/mL)	Vol. Standard[1] (μL)	Vol Buffer[2] (μL)	Vol Dye[3] (μL)
0	0	160	40
0.5	10	150	40
1	20	140	40
2	40	120	40
4	80	80	40
6	120	40	40
8	160	0	40

[1]Standard is 10 μg/mL BSA
[2]Buffer is 1X PBS
[3]Dye is the Bradford Reagent, Coomassie Brilliant Blue G-250

2) Create a standard curve by measuring the absorbance at 595 nm and plotting absorbance as a function of time.

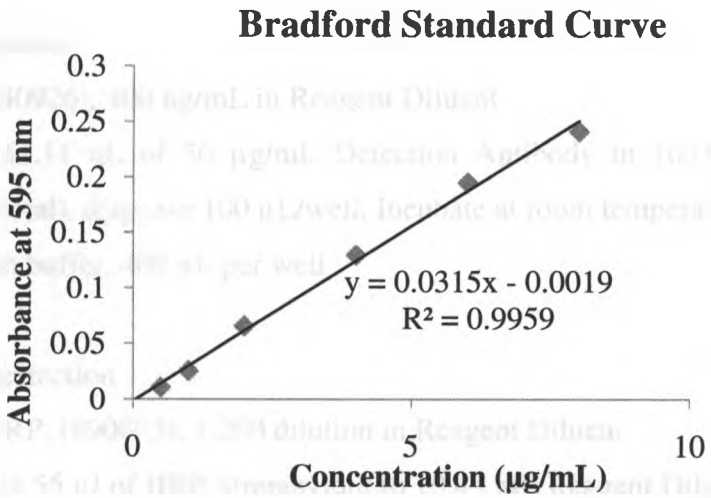

3) Perform a linear regression, and derive formula to solve for unknown concentration from absorbance.

4) Measure absorbance of samples and solve for the concentration.

Appendix F – Enzyme Linked Immunosorbant Assay (ELISA) Protocol

ELISA Protocol for PDGF-BB

Step 1: Coat

Capture Ab (840925), 0.4 µg/mL in PBS (1X)

For one plate, 61.11 uL of 72 µg/mL Capture Reagent in 10938.89 uL PBS (11 mL total), dispense 100 µL/well. Cover plate with parafilm and incubate at room temperature overnight (or in fridge up to one week). Wash 3X – Wash buffer, 400 µL per well

Step 2: Block

Reagent Diluent 300 µL per well. Incubate at room temperature for one hour. Wash 3X – Wash buffer, 400 µL per well

Step 3: Standards and samples

Dilute standards and samples in Reagent Diluent

Standard curve serially diluted (2-fold) from 2000 pg/mL, for 1 plate 12 µL of 110 µg/mL PDGF-BB (840927) in 648 µL Reagent Diluent. Dilutions are done in polypropylene plate and then transferred to polystyrene plate, 100 µL/well

Incubate at room temperature for two hours. Wash 3X – Wash buffer, 400 µL per well

Step 4: Biotinylation

Detection Ab (840926), 400 ng/mL in Reagent Diluent

For one plate, 61.11 uL of 50 µg/mL Detection Antibody in 10938.89 µL Reagent Diluent (11 mL total), dispense 100 µL/well. Incubate at room temperature for two hours

Wash 3X – Wash buffer, 400 µL per well

Step 5: Biotin dectection

Streptavidin – HRP, (890803), 1:200 dilution in Reagent Diluent

For one plate, add 55 µl of HRP Streptavidin to 10.45 mL Reagent Diluent (11 mL total), dispense 100 µL/well, Incubate at room temperature for 20 minutes. Wash 3X – Wash buffer, 400 µL per well

Step 6: Colour development

TMB kit, (R&D DY999 - in fridge), mix 5.5 mL vial A + 5.5 mL vial B, use immediately

100 µL per well, Incubate for 20 minutes

Step 7: Stop

2N H_2SO_4, add 27.75 mL 18N H_2SO_4 to 225.25 mL dH_20 (in acid cabinet)

50 µL per well pipetted in the same order as previous step. Read plate immediately

Step 8: Read

Microplate reader at 450 nm and at 540 or 570 nm (to subtract for correction)

Zero - read blank wells and set average value to first well

Step 9: Plot

Plot the absorbance difference ($ABS_{450} - ABS_{570/540}$) against known concentration using a four parameter logistic plot. Calculate concentration from sample absorbencies.

Appendix G – SDS-PAGE and Western Blotting

Total Protein Collection

Procedure:

1. Prepare fresh Lysis Buffer and put on ice.
2. 500 µg of each solid collagen was dissolved 400 µl of the lysis buffer.
3. Homogenized the samples with tissue homogenizer (Ultra Turrax T25 homogenizer, IKA Laboratory Equipment) for 2-3 minutes each
4. Sonicate the samples on ice (Model 500 Dismembrator, Fisher Scientific) for 20s total (in pulses of 5s on 2s off) at 30% amplitude.
5. Finally, heat the samples to 95 degrees C for 3 minutes to get all collagen into solution.

SDS-PAGE

Preparation:

1. Ensure all required buffers are made and are still good.
2. From the BCA protein counts, work out how many µl of sample must be loaded to load 50µg of protein.
3. Determine the size of proteins that will be probed for and decide what % of acrylamide is required for best resolution of those size proteins.

Procedure:

1. Take out protein samples and size standard to thaw on ice.
2. Clean Glass plates and combs. Clean and wipe plates with Windex, rinse residue with distilled water, and finally wipe clean with 70% alcohol. Wipe combs with alcohol to remove any old acrylamide.
3. Assemble gel apparatus as per manufacturer's instructions.
4. Prepare 1.5% APS fresh (0.15g per 10mL water)
5. Prepare 10mL Separating Gel per apparatus used

Component	6% gel (>100kDa)	8% gel (60-100kDa)	10% gel (40-60kDa)
1.5M Tris, pH 8.8	2.5 mL	2.5 mL	2.5 mL
10% SDS	200 µl	200 µl	200 µl

30% Acrylamide mix	2.0 mL	2.7 mL	3.3 mL
Autoclaved H_2O	4.64 mL	3.93 mL	3.33 mL
1.5% Ammonium Persulfate	655 µl	655 µl	655 µl
TEMED	5 µl	5 µl	5 µl

** mix solution gently by inversion before adding APS and again before adding TEMED. Invert gently a few times before pipetting between glass plates. Ensure 0.1% SDS overlay is ready to be added immediately.*

6. Quickly add acrylamide solution between plates via pipetting to approximately ½ cm below where the comb will sit. On the Mini-Protean 3 this is just to the bottom of the green cross bar behind the glass plates.
7. Immediately and gently overlay the acrylamide with 0.1% SDS buffer.
8. Allow gel to set for 45 minutes to an hour.
9. During gel hardening, prepare the loading samples (on ice):
   - Figure out which sample requires the most loading volume, and round up to the nearest multiple of 5. This volume figured is now the Loading Volume.
   - Prepare loading samples by taking the volume from the stock tube required for 50µg of protein (figured in Preparation step 2) and adding enough 1x Loading Buffer (in fridge) to bring up volume to the calculated Loading Volume.
   - Because the protein was boiled on collection it doesn't need to be boiled now. If the protein has not been boiled yet it can be heated at 95°C for 5 minutes and put on ice now.
10. Once the Separating Gel has hardened, pour off the SDS overlay and wash the top of the gel with water. Tip casting stand on its side to drain water and blot out any remaining water with folded paper towel. Allow gel to air dry while preparing the Stacking gel.
11. Prepare the Stacking Gel (one 5mL preparation enough for two stacking gels):

    830µl 30% acrylamide

    3.0mL autoclaved H_2O

    630µl 1.0M Tris, pH 6.8

    200µl 10% SDS

** mix solution gently at this point and add the following reagents one at a time, mixing gently by inversion between additions.*

332µl 1.5% APS

8µl TEMED

12. Quickly add Stacking gel to the remaining space on top of the Separating gels. Set the combs in place without introducing bubbles to the gel and allow to harden for 20 minutes.
13. Prepare 500mL of 1x Running Buffer per 2 gels (i.e. 500mL per tank).
14. Measure out protein size standards as per manufacturer's instructions (usually 5-10µl of stock standard per gel) and dilute with 1x Loading Buffer to the same loading volume as samples.
15. Once Stacking Gels are set, pull out the comb carefully and wipe out any waste acrylamide (it may be necessary to wash out the wells with Running Buffer to get any excess acrylamide clear of the wells). Detach from the casting stand and wipe away any excess gel. Assemble into the gel apparatus according to manufacturer's instructions. Fill inner tank with Running Buffer and check for leaks.
16. Load samples and ladders as far from the outside lanes as possible, loading 1x Loading Buffer in any unused wells.
17. Place apparatus in tank and fill outside with remaining Running Buffer. Place lid on (check polarity is correct) and connect leads to power pack.
18. Run at 130V for as long as it takes for protein of interest (tracked by position of size standards) to be in the bottom half of the gel (usually about an hour).
19. During the run, cut 1x nitrocellulose membrane and 4x Whatman filter paper per gel (size using spare plates or sponges). Prepare 1L 1x Transfer Buffer (+20% methanol) per 2 gels and chill at 4°C.
20. Once the run is complete, pour ~500mL of Transfer Buffer into each of 2 trays. Using a dull pencil, label the nitrocellulose membrane. In one tray soak one sponges, 3 filter papers and 1 nitrocellulose membrane (pre-wet this with water before placing in buffer). In the other tray place the sandwich apparatus with the black side down and place one sponge on the black side. Place one filter paper on top of the sponge.

Take out the gel apparatus and empty Running Buffer into the sink. Rinse out the tank with tap water.

21. Disassemble gel apparatus and carefully separate glass plates (keep the gel on the larger plate). Use a razor or a blunt scraper to remove the stacking gel from the separating gel.
22. Place a soaked piece of filter paper onto the gel as it sits on the larger plate (without introducing air bubbles if possible). Invert the plate and gently use the blade/scraper to ease the gel onto the filter paper. Place the filter paper and gel (with the well side pointing to the top of the apparatus) onto the sandwich apparatus.
23. Place the soaked nitrocellulose onto the gel label side facing the gel. Cover with two more filter papers and the remaining sponge.
24. With a broken plastic pipette, gently roll out any air bubbles from the stack. Then clamp the sandwich together and place into the other tray of buffer (i.e. keep it wet while preparing other transfers). Repeat steps for all remaining gels.
25. Once all sandwiches prepared, place into transfer apparatus with the black side of the sandwich facing the black half of the apparatus. Replace the top (ensuring polarity is correct) and place assembled tank into a Styrofoam ice box.
26. Pack the tank in ice and fill ice box with water to halfway up the tank. Run the transfer for 1 hour at 75V (alternatively, transfer can be done at 30V overnight while stirring the buffer, but there is a risk of transferring small proteins right through the membrane).
27. Once transfer is complete, disassemble and toss everything except for the nitrocellulose membrane. Cut this to the imprint of the gel along the top and bottom and place in 1x TBS. Two membranes can occupy the same dish of TBS, but cannot be facing each other (protein side must face out).
28. Once all membranes are collected, fill 3 containers with 1) Ponceau S solution, 2) Water and 3) TBS. Stain one blot at a time in Ponceau S (a few seconds is enough), then destain in water until bands can be seen. Note condition of the protein bands and apparent evenness of loading, and place blot in TBS to remove the stain.
29. Blots may be kept in TBS at 4°C for no more than 48 hours prior to Blotting.

Western Blotting

Preparation:

1. Make 1x TBS and 1x TBS-T (TBS + 0.05% Tween-20)
2. Make enough 5% non-fat dried milk (NFDM)(in TBS-T) for 30mL per blot.

Procedure:

1. Pour off TBS storage buffer and add 10mL NFDM to block non-specific binding. Rock for 1 hour at room temperature (rock across width of the blot not the length).
2. Make a dilution of primary antibody in 10 mL NFDM solution as appropriate (starting dilutions usually found on product sheets).
3. After blocking completed, pour off blocking solution and add milk containing primary antibody. Rock for 1 hour at room temperature or overnight at 4°C.
4. After 1 hour, pour off primary solution and wash 4x 5 minutes with TBS-T.
5. Prepare appropriate dilution of secondary antibody (1:10,000 usually a good starting point) in 10 mL NFDM.
6. After final TBS-T wash, add secondary solution and rock for 1 hour at RT.
7. After incubation, wash 3x 5 minutes with TBS-T and 1x 5 minutes with TBS.
8. During TBS wash prepare 10mL of Supersignal for every 2 blots (according to manufacturer's instructions).
9. Pour TBS from half of the containers and add Supersignal solution. Rock 5 minutes. Once complete, pour TBS off the remaining half of the blots and pour in the used Supersignal solution (i.e. one 10mL preparation of Supersignal is enough to treat two separate blots). Incubate for 5 minutes
10. Immediately wrap the first set of blots in Saran Wrap to preserve Supersignal, while the second set incubates.
11. Once the second set of blots is ready, remove them from Supersignal (keep the solution though in case you need to rewet the membrane) and shake off the excess solution. Wrap immediately in Saran Wrap.

Appendix H – Supplementary PEG Data

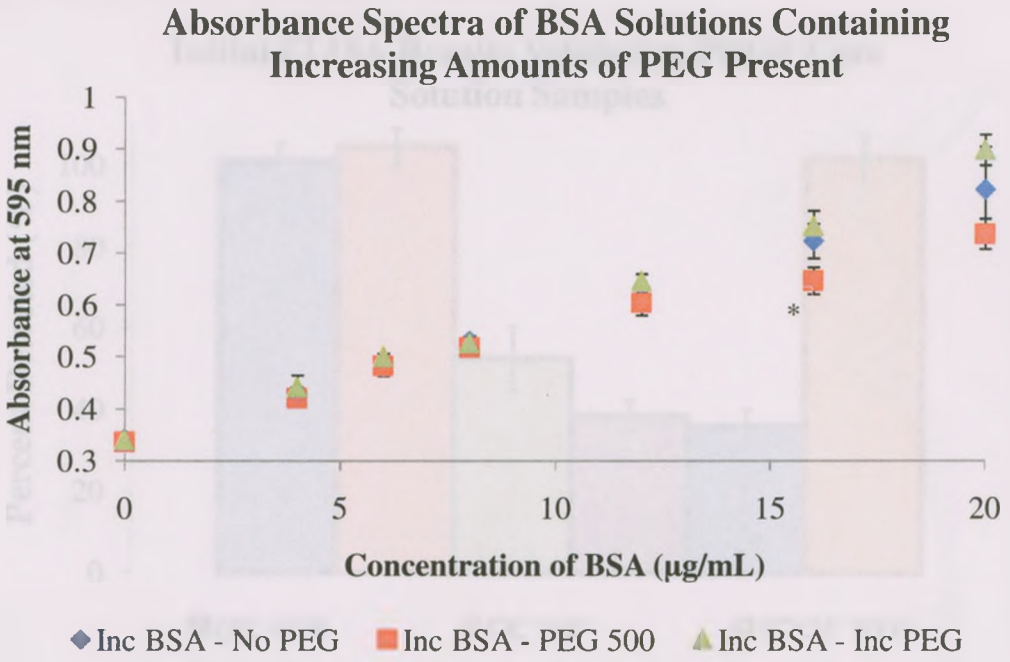

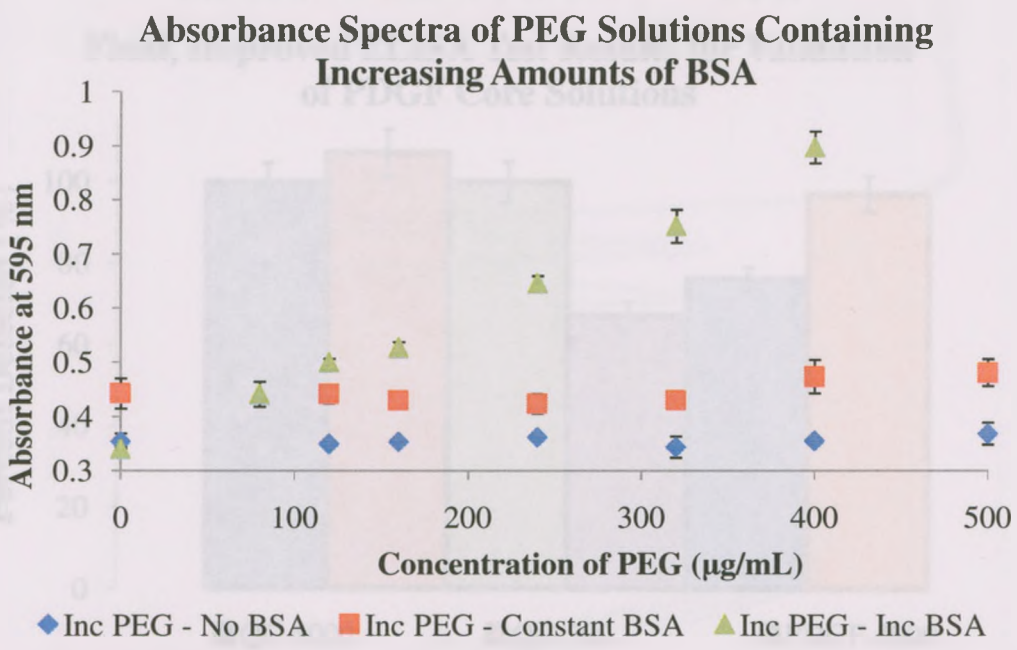

Influence of PEG on BSA Absorbance: Samples were analyzed using Bradford Assay to determine concentration of BSA detected. Only one data point showed a significant difference between the control (No PEG) samples with 500 µg/mL PEG ($p = 0.0158$). PEG solutions demonstrated no significant increases in absorbance without the presence of BSA. (Legend: Inc BSA – Increasing BSA from 0-25 µg/mL, No PEG – 0 µg/mL PEG, PEG 500 – 500 µg/mL PEG, Inc PEG – Increasing PEG from 0-400 µg/mL, No BSA – 0 µg/mL BSA, Constant BSA – 4 µg/mL).

Appendix I – Preliminary ELISA Data

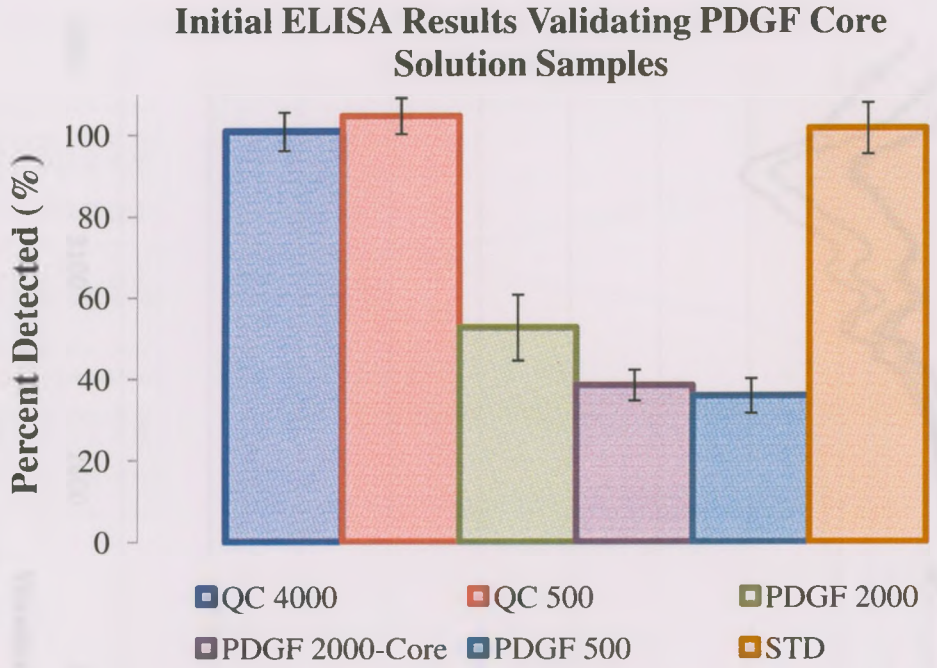

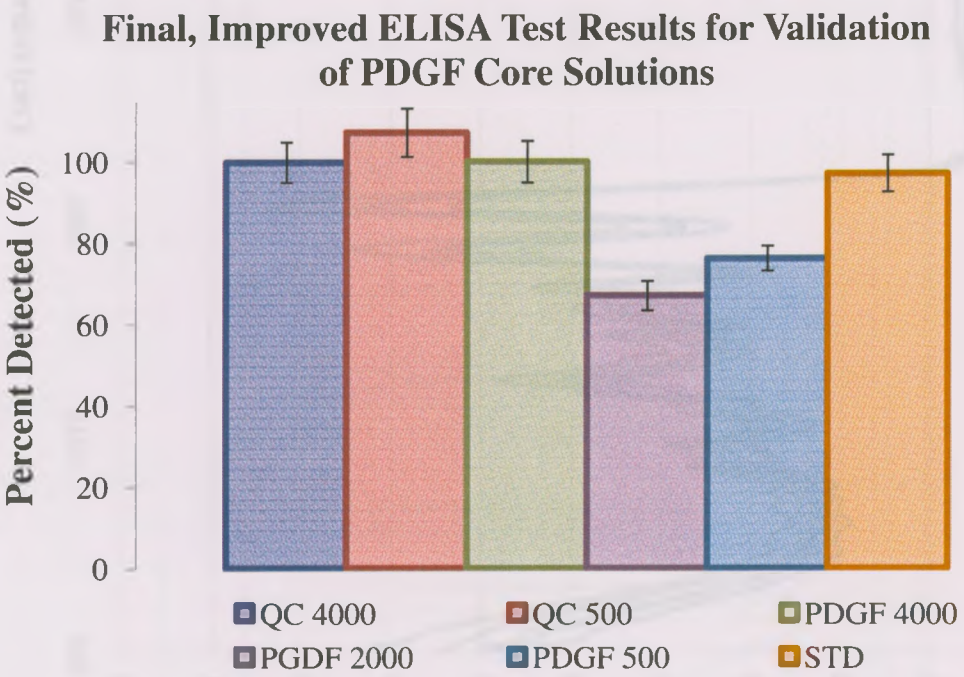

Comparison of ELISA DATA: Samples were analyzed using ELISA to determine sample concentration. As can be seen, initial results were only recovering ~50 % of PGDF purchased. After several troubleshooting efforts, sample concentrations and accuracy of ELISA was improved to ~ 80 % (Legend: QC – Quality Control, PDGF-Sample, STD – Standard, 500 - 4000 – Concentration in pg/mL).

Appendix J – IR Spectra for Multiple Collagen Samples

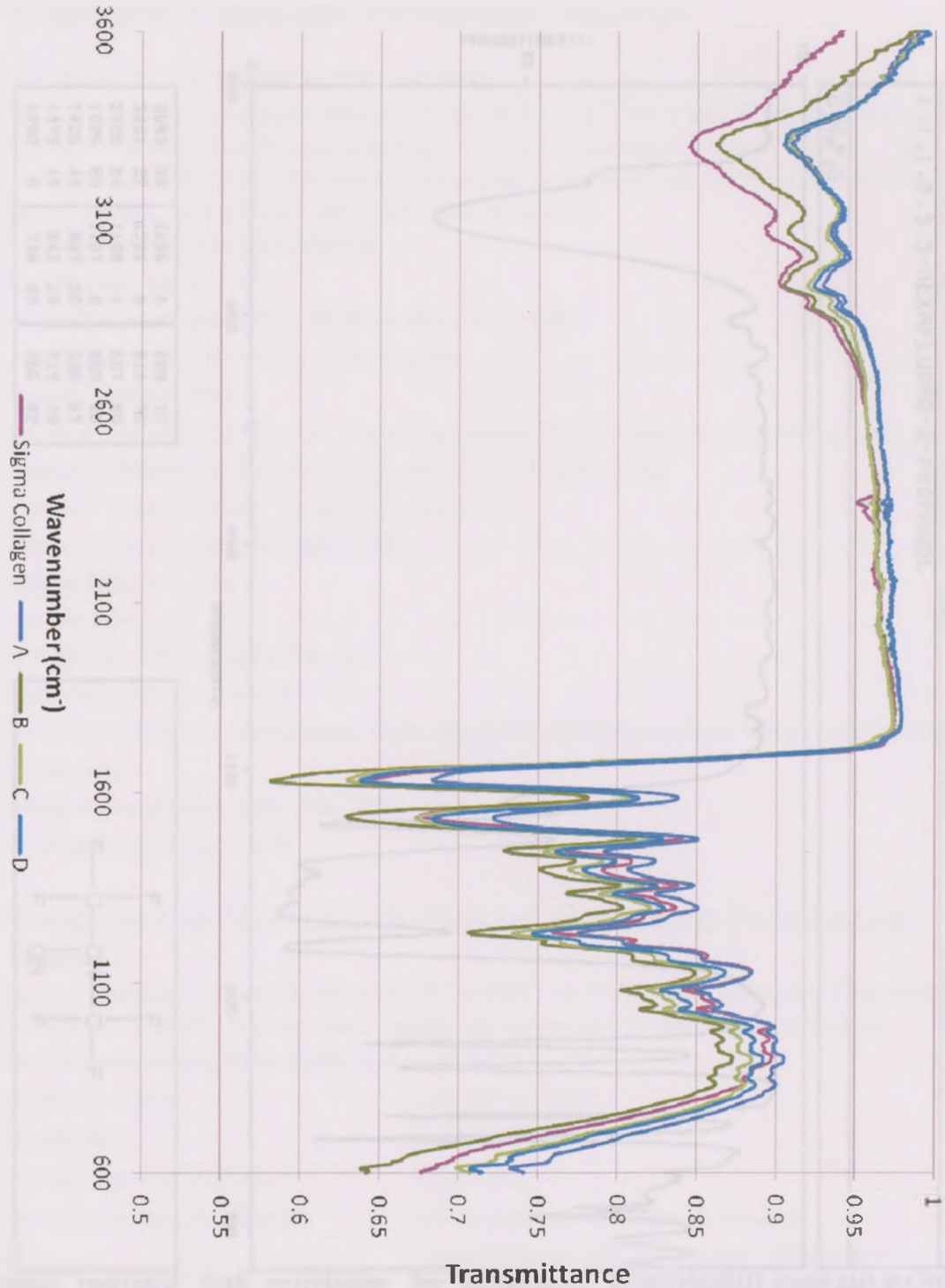

Appendix K – IR Spectra for Hexafluoroisopropanol (HFIP)

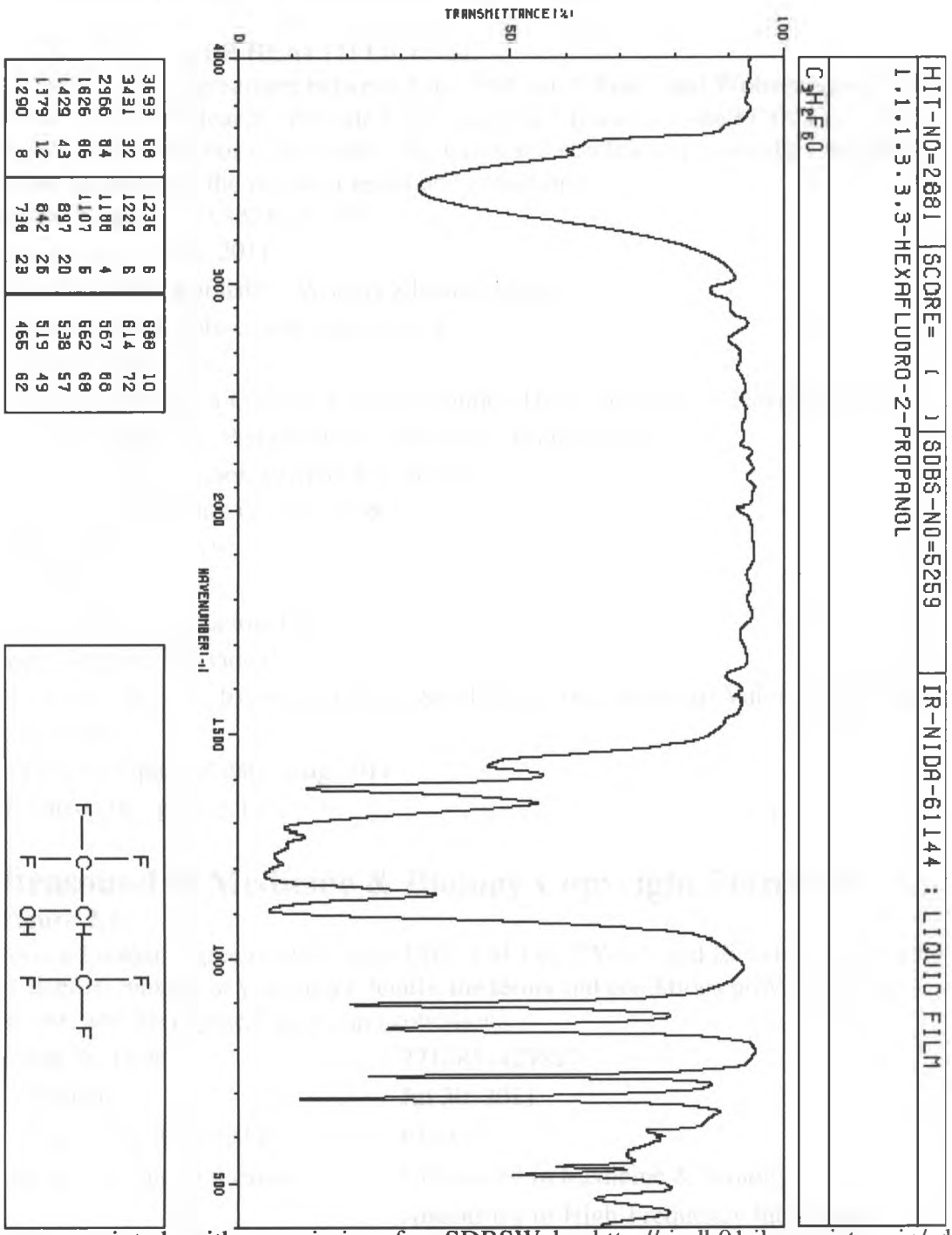

Image reprinted with permission for SDBSWeb: http://riodb01.ibase.aist.go.jp/sdbs/ (National Institute of Advanced Industrial Science and Technology, July 10, 2011)

Appendix L – Copyright Permissions

Circulation Copyright Permission – Figure 2.1

WOLTERS KLUWER HEALTH LICENSE
This is a License Agreement between Erica EM Lee ("You") and Wolters Kluwer Health ("Wolters Kluwer Health") provided by Copyright Clearance Center ("CCC"). The license consists of your order details, the terms and conditions provided by Wolters Kluwer Health, and the payment terms and conditions.
License Number: 2704351326508
License date: Jul 08, 2011
Licensed content publisher: Wolters Kluwer Health
Licensed content publication: Circulation
Licensed content title:
Evolving Concepts of Cardiac Valve Dynamics:The Continuum of Development, Functional Structure, Pathobiology, and Tissue Engineering
Licensed content author: Frederick J. Schoen
Licensed content date: Oct 28, 2008
Volume Number: 118
Issue Number: 18
Type of Use: Dissertation/Thesis
Requestor type: Individual
Title of your thesis / dissertation: Core-Shell Nanofibres for Heart Valve Leaflet Tissue Engineering
Expected completion date: Aug 2011
Estimated size (pages):100

Ultrasound in Medicine & Biology Copyright Permission – Figure 2.2

This is a License Agreement between Erica EM Lee ("You") and Elsevier ("Elsevier"). The license consists of your order details, the terms and conditions provided by Elsevier, and the payment terms and conditions.

License Number	2718851427827
License date	Jul 30, 2011
Licensed content publisher	Elsevier
Licensed content publication	Ultrasound in Medicine & Biology
Licensed content title	Anisotropy of High-Frequency Integrated Backscatter from Aortic Valve Cusps
Licensed content author	Zamir Khan,Derek R. Boughner,James C. Lacefield
Licensed content date	September 2008

Licensed content volume number	34
Licensed content issue number	9
Number of pages	9
Type of Use	reuse in a thesis/dissertation
Portion	figures/tables/illustrations
Number of figures/tables/illustrations	1
Format	print
Are you the author of this Elsevier article?	No
Order reference number	
Title of your thesis/dissertation	Core-Shell Nanofibres for Heart Valve Leaflet Tissue Engineering
Expected completion date	Aug 2011
Estimated size (number of pages)	100

Macromolecular Chemistry and Physics Copyright Permission – Figure 2.6

This is a License Agreement between Erica EM Lee ("You") and John Wiley and Sons ("John Wiley and Sons"). The license consists of your order details, the terms and conditions provided by John Wiley and Sons, and the payment terms and conditions.

License Number	2718350054133
License date	Jul 29, 2011
Licensed content publisher	John Wiley and Sons
Licensed content publication	Macromolecular Chemistry and Physics
Licensed content title	Ultrafine Electrospun Polyamide-6 Fibers: Effect of Solution Conditions on Morphology and Average Fiber Diameter
Licensed content author	Chidchanok Mit-uppatham,Manit Nithitanakul,Pitt Supaphol
Licensed content date	Nov 26, 2004
Start page	2327
End page	2338
Type of use	Dissertation/Thesis
Requestor type	University/Academic
Format	Print
Portion	Figure/table
Number of figures/tables	1
Original Wiley figure/table number(s)	Figure 2